JOURNAL OF GEOPHYSICAL RESEARCH, VOL. 104, NO. D24, PAGES 31,301–31,320, DECEMBER 27, 1999

Comparisons between buoy-observed, satellite-derived, and modeled surface shortwave flux over the subtropical North Atlantic during the Subduction Experiment

Duane E. Waliser

Institute for Terrestrial and Planetary Atmospheres, State University of New York, Stony Brook

Robert A. Weller

Woods Hole Oceanographic Institution, Woods Hole, Massachusetts

Robert D. Cess

Institute for Terrestrial and Planetary Atmospheres, State University of New York, Stony Brook

Abstract. Two years of surface shortwave flux data, from five buoys in the subtropical North Atlantic Ocean during the Subduction Experiment, were used to examine shortwave absorption in the atmosphere, and its partitioning between the clear and cloudy sky. Robust methods were used to isolate the clear-sky shortwave observations so that they could be directly compared to values derived using a single-column version of the National Center for Atmospheric Research Community Climate Model radiation code. The model-derived values agreed with the observations to within 0.5% mean relative error. Additional analysis showed that the model-data clear-sky surface shortwave differences showed no systematic relationship with respect to column water vapor amount. These results indicate that clear-sky absorption of shortwave radiation appears to be well modeled by current theory. Model-derived clear-sky surface shortwave values were combined with the observed (all-sky) values to determine the surface shortwave cloud forcing. The mean of these series were combined with 5-year mean Earth Radiation Budget Experiment derived top of the atmosphere (TOA) cloud forcing values to estimate the surface to TOA cloud forcing ratio. The resulting values range between 1.25 and 1.59. These values, along with the agreement between modeled and observed clear-sky surface shortwave, support the suggestion that our current theoretical radiative transfer models do not properly account for the amount of shortwave energy absorbed by the cloudy atmosphere. Mean values from the 2-year shortwave flux time series were compared to mean values from two climatologies derived from bulk parameterizations that utilize ship-based cloud reports. These comparisons show that the Oberhuber climatology underestimates the surface shortwave flux by ~20% (~40 W m^{-2}), while the Esbensen and Kushnir climatology underestimates the flux by ~4% (~8 W m^{-2}). The observed mean values were also compared to five satellite-derived climatologies. These comparisons showed much better and more consistent agreement, with relative bias errors ranging from about -1 to 6%. Comparisons to contemporaneous, daily-average satellite derived values show relatively good agreement as well, with relative biases of the order of 2% (~3-9 W m^{-2}) and root-mean-square differences of ~10% (25-30 W m^{-2}). Aspects of the role aerosols play in the above results are discussed along with the implications of the above results on the integrity of open-ocean buoy measurements of surface shortwave flux and the possibility of using the techniques developed in this study to remotely monitor the operating condition of buoy-based shortwave radiometers.

1. Introduction

In most regions of the globe, solar energy is a significant part of the surface energy budget and in most instances it accounts for most, if not all, of the positive heat flux transferred across the air-sea interface from the atmosphere to the ocean. In this regard, the significance of solar energy in the climate system is undeniable, and a substantial amount of effort has been undertaken to correctly account for this energy in numerical weather forecasting and climate simulations/predictions. This is an especially difficult endeavor due to the complex nature of clouds which, aside from the diurnal and annual cycles, provides the largest spatial and temporal modulation to shortwave radiation in the climate system [*e.g., Cess et al.,* 1989; *Harrison et al.,* 1990; *Arking,* 1991]. The difficult nature of this task is outweighed only by its importance due to the fact that our lack of understanding of clouds represents the single largest uncertainty in assessing the impact of anthropogenic changes on the Earth's climate system [*Intergovernmental Panel on Climate Change (IPCC),* 1995].

Paper number 1999JD900946.
0148-0227/99/1999JD900946$09.00

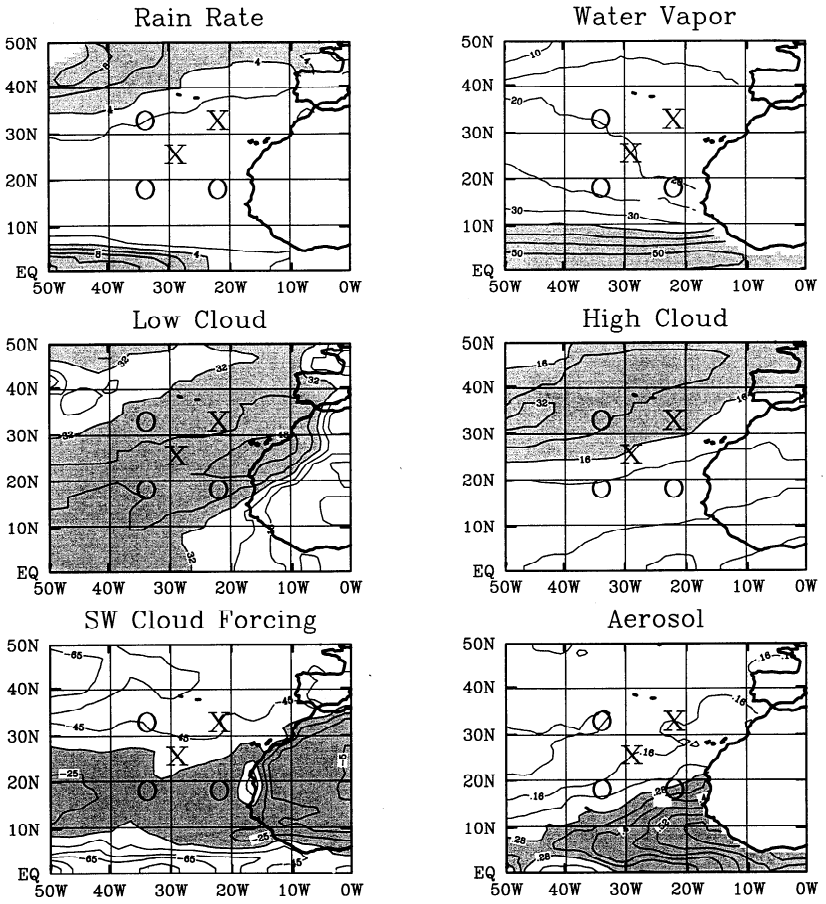

Figure 1. February means of rain rate (top left, mm d^{-1}), precipitable water (top right, mm), low-cloud frequency (middle left, percent), high-cloud frequency (middle right, percent), shortwave cloud forcing at the top of the atmosphere (bottom left, W m^{-2}) and aerosol optical thickness (bottom right, unitless). See Introduction section for data sources. Crosses (open circles) mark the locations of the two discus (three toroid) buoys (see section 2).

One significant limitation in pursuing the above line of research is the lack of shortwave validation data readily available at the surface of the ocean. Having such validation data is critical owing to the large area of the planet's surface covered by ocean and because ocean regions often exhibit atmospheric conditions (e.g., cloud types, aerosol characteristics, water vapor profiles) different from their continental counterpart. Until the introduction of radiation sensors to the TOGA TAO buoys [*McPhaden,* 1995; *Kessler and McPhaden,* 1995; *Zhang et al.,* 1995; cf. *Servain et al.,* 1998], time series of surface shortwave data from the ocean had been limited to a few isolated and relatively short (weeks to months) surface mooring deployments (e.g., Frontal Air-Sea Interaction Experiment (FASINEX) [*Weller,* 1991], BioWatt [*Dickey et al.,* 1993], Marine Light Mixed Layer Experiment (MLML) [*Plueddemann et al.,* 1995], Coupled Ocean Atmosphere Response Experiment (COARE) [*Weller and Anderson,* 1996]). One exception is the Subduction Experiment [*Brink et al.,* 1995; *Moyer and Weller,* 1997] which was conducted over a 2-year period, from June 1991 to June 1993, in the subtropical North Atlantic. This experiment included five moorings spanning 15° in latitude and 12° in longitude off the west coast of Africa. Figures 1 and 2 show the geographic locations of these buoys superimposed on February and August mean maps of several radiatively important quantities: rain rate from the Microwave Sounding Unit (MSU; 1979-1993 *[Spencer,* 1993]) precipitable water from Special Sensor Microwave Imager (SSM/I; 1987-1995 [*Ferraro et al.,* 1996]), low and high cloud frequencies from the International Satellite Cloud Climatology Project (ISCCP; 1983-1990 [*Rossow and Schiffer,* 1991]), shortwave cloud forcing at the top of the atmosphere from the Earth Radiation Budget Experiment (ERBE; 1985-1989 [*Barkstrom,* 1984]), and aerosol optical depth from the Advanced Very High Resolution Radiometer (AVHRR; 1988-1995 *Stowe et al.,* 1997]). Figures 1 and 2 illustrate the atmospheric climate(s) regime sampled by the Subduction Experiment. In general, this region is characterized by very little mean rainfall (< 2 mm d^{-1}), significant low-level cloudiness (~30 - 50%), and moderate shortwave cloud forcing (~ -25 – -50 W m^{-2}). Taking into account the spatial distribution of the moorings and the variability of the annual cycle, the sampling also includes very dry to relatively moist conditions (~15 – 45 mm), pristine air to air heavily laden with atmospheric aerosol (i.e., Saharan dust), and regions with virtually no high clouds (< 8%) and others with modest amounts (~25%) associated with midlatitude synoptic variability.

Given the Subduction Experiment's unique and potentially valuable record of surface shortwave observations,

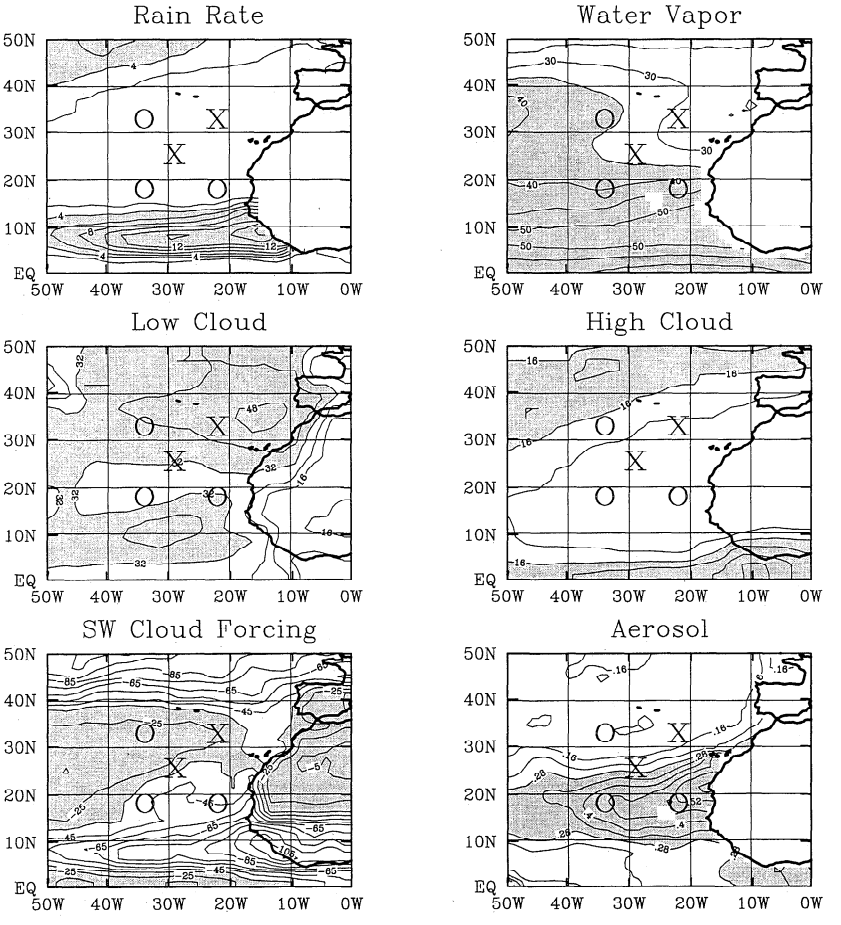

Figure 2. Same as Figure 1, except for August means.

the purpose of this study is to analyze and exploit these data in order to address a number of important questions regarding the measurement, modeling, and understanding of shortwave radiation in our climate system. The first question involves the recent debate concerning clear-sky shortwave absorption and how well this quantity is predicted by theoretical radiative transfer models (e.g., radiation parameterization in a typical general circulation model (GCM)). Studies by *Charlock and Alberta* [1996], *Arking* [1996], *Imre et al.* [1996], and *Kato et al.* [1997] all suggest that models may be underestimating the amount of clear-sky shortwave radiation absorbed by the atmosphere. Another set of studies, including those by *Cess et al.* [1996], *Conant et al.* [1997], *Zender et al.* [1997], *Chou and Zhou* [1997], and *Jing and Cess* [1998], find good agreement between model-predicted and observed clear-sky shortwave radiation. Most of the data sources used in the studies cited above tend to be limited to relatively short tropical ocean time series (e.g., COARE) or midlatitude land-based time series (e.g., Atmospheric Radiation Measurement (ARM) Oklahoma site). Addressing the same question using the long-running, subtropical ocean data set from the Subduction Experiment provides a unique set of complimentary data and associated conclusions.

A second question that can be addressed with the Subduction Experiment data hinges on the result of the first question. If indeed there is good model-data agreement found for the clear-sky observations, then the model can be used to generate the expected clear-sky surface shortwave time series at the five mooring sites. From the measured all-sky time series and the model-derived clear-sky time series, the surface shortwave cloud forcing can then be determined. The mean value of this quantity can be compared to the mean top of the atmosphere (TOA) shortwave cloud forcing derived from ERBE to estimate the extent that the cloudy atmosphere absorbs shortwave radiation. The amount of absorption has been the subject of significant debate recently, as a number of authors have noted that observations show that the TOA to surface ratio of shortwave cloud forcing has a value of ~1.2-1.5 [e.g., *Ramanathan et al.*, 1995; *Cess et al.*, 1995; *Pilewskie and Valero*, 1995; *Waliser et al.*, 1996], while a typical GCM yields values somewhere near 1.1 [e.g., *Cess et al.*, 1996; *Zender et al.*, 1997; *Wild et al.*, 1995; *Kiehl et al.*, 1995]. As with the above question regarding clear-sky absorption, little data from the open oceans and virtually no data from the subtropics have been applied to this problem.

Finally, while it has become relatively routine to derive the surface shortwave flux from satellites [e.g., *Gautier*, 1980; *Wang*, 1994; *Li et al.*, 1993a; *Bishop and Rossow*, 1991; *Pinker and Laszlo*, 1992, *Darnell et al.* 1992; *Zhang et al.* 1995], the lack of open-ocean insitu surface shortwave observations along with the uncertainties posed above warrant continued and further validation of these products (Data sets based on the *Pinker and Laszlo* [1992] and *Darnell et al.* [1992] methods are described by *Whitlock et al.* [1995]). To date, most validations over the ocean have consisted of climatologies based on bulk algorithms using

ship reports [e.g., *Weare et al.,* 1980; *Esbensen and Kushnir,* 1981; *Oberhuber,* 1988]. While such climatologies can be useful for a general description of surface shortwave variability, their validation against actual radiometer measurements has been tenuous. *Weare* [1989] has shown that due to the uncertainties in the bulk formulas and their sparse sampling, it is probably conservative to associate (spatially dependent) errors of the order 30-70 W m^{-2} with these methods. In this respect, these data are not adequate to serve as robust validation for satellite retrievals over the open ocean.

Validation to date besides the ship data has largely consisted of land-based data, such as the GEBA [*Ohmura and Gilgen,* 1991], the Baseline Surface Radiation Network (BSRN) [*Ohmura et al.,* 1998], and a number of field experiments (e.g., First ISCCP Regional Experiment (FIRE), ARM). For example, the *Li et al.* [1993a] retrieval has been compared to tower data [*Li et al.,* 1993b]; and both the *Pinker and Laszlo* [1992] and *Li et al.* [1995] data have been compared to the GEBA data set [*Li et al.,* 1995], the latter of which consists of monthly means of land and, in a few cases, island stations. In one notable exception, *Bishop et al.* [1997] have compared satellite retrievals to a set of island stations as well as to buoy time series from the MLML (~4 months) and BioWatt (~9 months) experiments. Their comparisons to the buoy time series, based on daily values, were somewhat mixed, with biases ranging between +18 to −9 W m^{-2}, and root-mean-square differences on the order of 25-40 W m^{-2}. Interestingly, their analysis of the island stations revealed that many of the island stations inadequately represent open ocean conditions due to orographic-induced biases. These biases, combined with the rarity of true open-ocean surface shortwave records, represent a limitation to the accuracy, or at least the confidence, which can be attributed to the satellite retrievals. Yet these retrievals are likely to be the best generalized method for diagnosing the role and variability of solar energy at the ocean surface, validating GCM representations of surface solar heat flux, as well as providing surface shortwave boundary conditions for ocean model simulations [e.g., *Seager and Blumenthal,* 1994; *Waliser et al.,* 1994; *Murtagude and Busalacchi,* 1998]. Therefore it is crucial that every available record of insitu shortwave flux be exploited to help constrain the uncertainties surrounding satellite retrievals of surface shortwave flux.

In the following section, we describe the buoy observations from the Subduction Experiment in more detail and briefly discuss other sources of data used in this study. In section 3, we describe the methods behind, and results of, the model versus observed clear-sky surface flux comparisons. In section 4, we consider all-sky aspects of the buoy observations, such as the implied surface shortwave cloud forcing and its comparison to TOA values. In section 5, we examine the agreement of ship and satellite-based shortwave values to the buoy-observed values. In section 6, we summarize the results and discuss the implications of the results on future observation efforts.

2. Data

2.1. Buoy

The five Subduction moorings were deployed from June 1991 to June 1993 as part of the cooperative Subduction and Atlantic Stratocumulus Transition Experiments (ASTEX). The Subduction experiment sought to understand the process that leads surface water in the subtropical North Atlantic to be carried down into the interior of the ocean on seasonal to annual timescales. To do this, a widely spaced array was required, as it was desirable to both observe the convergence of the Ekman flow by the winds associated with the eastern end of the Azores high and to span the annual meridional migration of the surface outcrops of constant density surfaces. For ASTEX, a surface mooring was needed close to the Azores to provide a long-running time series of the air-sea fluxes that began 1 year before the intensive field phase and would provide the opportunity to examine relationships between cloud type and amount and sea surface temperature (SST) variability. These requirements were met by setting a large square array that also contained a central site. The corners of this array were located at 33°N, 34°W; 33°N, 22°W; 18°N, 34°W; and 18°N, 22°W, and the central site was located at 25.5°N and 29°W. Hereafter, these locations will be referred to as northwest, northeast, southwest, southeast and central, respectively. Actual locations varied by up to 6 min for the three different deployments for each buoy. Exact locations can be found in the work of *Brink et al.* [1995].

The strategy for obtaining 2 years of data from this array was to make three consecutive, 8-month deployments of surface moorings at each of the five sites. This was planned in order to minimize degradation in the performance of the meteorological sensors on the buoys due to exposure and the loss of oceanographic data due to biofouling. At each deployment, freshly calibrated meteorological sensors were used, and the recovered sensors were preserved intact for postdeployment calibration. Each buoy carried two, redundant meteorological instruments, a Vector Averaging Wind Recorder (VAWR) [*Weller et al.,* 1990] and an Improved Meteorological recorder (IMET) [*Hosom et al.,* 1995]. Both instruments measured barometric pressure, wind speed and direction, relative humidity, and incoming shortwave and longwave radiation. The IMET also measured precipitation. IMET recorded 1-min averages, and the VAWR recorded 15 min averages.

The discussion here will focus on the shortwave radiation sensors; *Moyer and Weller* [1997] provide further discussion of the VAWR and IMET and their sensors as deployed in the Subduction array. The 3-m diameter discus buoys used at northeast and central moorings and the 2.3-m diameter toroid buoys used at northwest, southwest, and southeast moorings were fitted with 2-m-tall, white, aluminum towers. The shortwave radiometers were placed at the uppermost position, at 3.5 m above the waterline, and had an unobstructed, hemispherical view of the sky. The VAWR was deployed with an Eppley 8-48 shortwave radiometer. The voltage output from the thermopile of the 8-48, proportional to the temperature difference between adjacent black and white segments of the sensor's surface, was amplified and digitized, with 15-min averages of this signal being recorded. The IMET was deployed with an Eppley Precision Spectral Pyranometer (PSP) as a shortwave sensor. The voltage from the PSP, proportional to the temperature difference between its all-black sensor surface and a thermistor in its base, was digitized every 2 s, and a 1-min average of this signal was recorded.

Particular care was taken during the preparation, deployment, and recovery of the shortwave sensors to address possible errors and calibration issues. Before the deployment,

the 8-48 and PSP shortwave sensors were returned to Eppley for calibration. Once calibrated, and after the gains of the amplifiers used with them were also checked, they were fitted to the instruments and the instruments were mounted on the buoy hulls. All systems on the buoy hulls, including the transmitters used to telemeter data via ARGOS, were powered up; and the buoys were placed in a field next to each other and next to a tower with a reference set of sensors. The shortwave radiation data from the five buoys was then closely checked for consistency among the five buoys and with the reference sensor and also for any evidence that radio frequency energy from the satellite transmitters was exciting the radiometers. On rare occasions, such evidence was found, and the radio frequency interference was removed by moving the transmitter's antenna to a different location on the buoy hull. Upon recovery and while on the deck of the ship during daylight hours, the shortwave radiometers were covered with an opaque plastic bag, providing a timing mark (the VAWR and IMET keep time to within one sample interval over 8 months) and preserving the condition of the radiometers. When the sensors were returned to Woods Hole Oceanographic Institution (WHOI) they were again sent to Eppley for calibration, first "as is," with any salt spray and dirt, and then after the quartz domes were washed. The 1-min PSP samples were averaged to 15-min for comparison to the 8-48 series, of which the latter data were used preferentially due to the second author's longer history and greater familiarity with the VAWR. However, when data from both the 8-48 and PSP were available, they were compared for indications of data quality problems in the 8-48 series. Significant differences between the two sensor series were limited to data from only two of the 15 8-month deployments. In these cases, the results of this quality check, together with the physical inspection of the sensors and comparison of postdeployment calibrations with the predeployment calibrations pointed to shifts in sensor calibration or to moisture inside the dome radiometer as the source of the problem. In these instances, the PSP series were used instead of the 8-48; this occurred on the first deployment of NE and the second deployment of NW buoys.

Calibration histories, including operating temperature dependencies, of each shortwave sensor have been maintained since purchase and through subsequent field deployments. Differences between "dirty" and "clean" calibrations have been 2% and less, within the standard deviation of all of the calibrations done on each sensor over the years, which is close to 3%. Beginning in 1992, in conjunction with TOGA COARE, the radiometers have also been sent to a standards laboratory for verification of the manufacturer's calibration. Prior to COARE, an accuracy of 5% was associated with the shortwave radiation measurements in the field. Extensive comparisons and calibrations done in conjunction with COARE [*Weller and Anderson,* 1996] showed that typical instantaneous accuracy was 3%, including other error sources in addition to calibration, such as buoy motion. In COARE, the error in the monthly mean shortwave was reduced further by using a calibration based on the COARE intercomparisons rather than relying on the manufacturer's calibration. These intercomparisons were not done in Subduction, and *Moyer and Weller* [1997] used 3% to determine an accuracy of 5 - 7 W m^{-2} in annual means of the net shortwave from the Subduction array.

Buoy motion and inclination is a possible source of error [*MacWhorter and Weller,* 1991]. The pitching and rocking of the buoy hull is small, as the tension (~1000 kg) in the mooring line provides a large righting moment. For both the toroid and discus buoys, the mooring line is attached to a rigid bridle on the underside of the buoy hull using a single mount point. The sensors are mounted level (to within ~1°) with the waterline of the buoy hull, and visual observations of the deployed buoy hulls suggest that they ride close to vertical. *MacWhorter and Weller* [1991] used buoy hull motion data collected in an earlier experiment to study the error and concluded that the error associated with pitch and roll was reduced in averages and that the mean tilt could introduce error of a similar magnitude. These error sources, and their differences with respect to the toroid and discus hulls used in this experiment, will be discussed again later in the paper.

Another consequence of buoy motion associated with surface gravity waves is the potential for rapid fatigue of mooring line components and subsequent failure of the mooring line. The Subduction experiment was conducted at a point when there was much to be learned about the design of long-lived surface moorings. This resulted in a number of mooring failures, especially in the first deployment. The northwest, southwest, and southeast buoys went adrift and were recovered early, leading to the data gaps seen in time series of the daily-averaged downwelling shortwave radiation from the moored array (Figure 3). In these cases, it was found that the mooring line, not the bridle, was the cause of the failure. In addition to the mooring failures that produced the gaps in the shortwave data, there are also short gaps in the barometric pressure, air temperature, and relative humidity time series due to sensor failures [see *Moyer and Weller,* 1997].

2.2. Other Sources

Additional sources of data include ISCCP DX cloud data which were used to isolate clear-sky buoy observations for comparison to model-derived values. The DX version of ISCCP consists of a pixel-level retrieval analysis at the resolution of the ISCCP B3 product [*Rossow and Schiffer,* 1991; *Rossow et al.,* 1996]. Details concerning the specific quantities used from this data set will be discussed in the next section. Precipitable water vapor time series for each buoy were obtained from Defense Meteorological Satellite Program (DMSP) SSM/I measurements and the algorithm of *Wentz et al.* [1986]. The SSM/I orbital/swath data were composited into daily maps with 0.5° spatial resolution, and the buoy time series were taken from the grid points nearest the mooring locations. The values in these daily maps typically consist of the average of ascending and descending (e.g., 0600 and 1800 LT) swath values. However, since the satellite/sensor does not sample the entire globe in a single day, these daily maps have missing areas which progress around the globe with time and account for intermittent missing data in the precipitable water time series. The amount of missing data in these water vapor time series will be discussed in the next section in association with Tables 2 and 4. The water vapor data, along the zonally averaged ozone climatology of *Grose and Gille* [1996], were used in the single-column radiation model to diagnose clear-sky surface radiation values (see section 3.2).

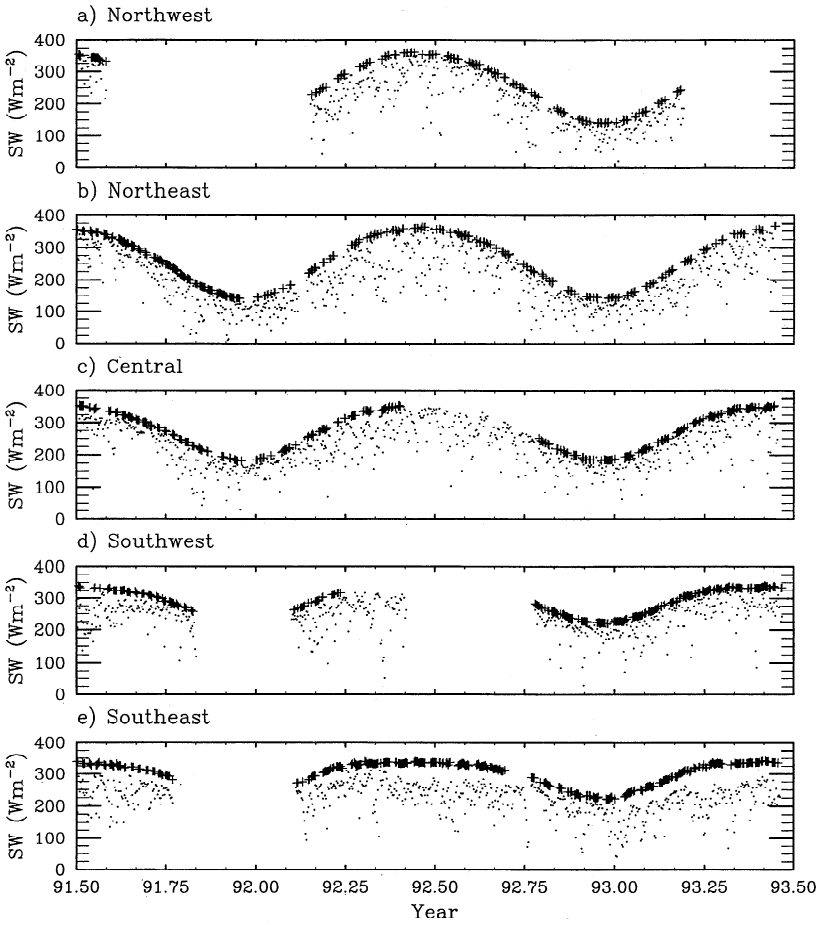

Figure 3. Daily mean surface shortwave values (dots) measured by the five Subduction Experiment buoys. Daily mean clear-sky surface shortwave values (crosses) computed by the model (see section 3). See Figure 1 or section 1 for latitude and longitude coordinates of the five mooring locations.

Two sets of daily aerosol retrievals were obtained to diagnose aerosol variability. The first is based on the Advanced Very High Resolution Radiometer (AVHRR) and the algorithm of *Stowe et al.* [1997]. The Stowe et al. method uses the upward scattered 0.63-μm channel radiance from AVHRR in cloud-free conditions, along with a radiative transfer model that accounts for the radiative properties of an assumed aerosol type, along with the contributions from Rayleigh and surface scattering and ozone absorption, to determine the aerosol optical thickness. The assumed aerosol type is best characterized as a conservatively scattering marine aerosol. Aerosol time series colocated with each buoy were constructed from the (1° x 1°: latitude x longitude) grid locations nearest each of the buoys. Since this agorithm is based on AVHRR visible satellite radiances, there are missing (daily) values associated with the presence of clouds. The second aerosol product is based on the Nimbus 7 Total Ozone Mapping Spectrometer (TOMS) and the algorithm of *Herman et al.* [1997]. This method uses the spectral contrast between the 0.34- and 0.38-μm channel radiances to detect the presence of ultraviolet (UV) absorbing aerosols (e.g., dust, smoke, volcanic ash, etc.). Note that this product does not provide a direct measure of aerosol thickness but instead computes a "N-value residue" that is more appropriate in this context to simply consider as a relative aerosol index. As with the AVHRR product, aerosol time series colocated with each buoy were constructed from the (1° x 1.25°: latitude x longitude) grid locations nearest each of the buoys. While the Herman et al. algorithm is based on TOMS UV absorption, and thus is much less sensitive to clouds, there is still missing data associated with interorbit gaps and heavy clouds.

Several surface shortwave data sets were obtained in order to compare them to the buoy-observed values. Two of these data sets are monthly climatologies that derive ocean surface shortwave from ship-based cloud reports and bulk parameterizations. These include the data sets from *Oberhuber* [1988] and *Esbensen and Kushnir* [1981, hereinafter referred to as EK]. The other data sets used in the comparison are satellite-derived products. These include monthly data sets based on the methods of *Gautier et al.* [1980; see also *Wang,* 1994], *Li et al.* [1993a], *Bishop et al.* [1997], *Zhang et al.* [1995] and *Darnell et al.* [1992]. In most cases, these data have been derived from ISCCP data with the exception of the Li et al. product that was derived from ERBE observations. Note that the ship-based and Li et. al. data sets provide net surface shortwave. For these cases, the data were converted to incoming shortwave using an ocean albedo of 0.06 [*Payne,* 1972]. Since none of the shortwave data sets described above include data contemporaneous with the Subduction Experiment, only comparisons based on long-term means, computed from 12-month annual cycles, were performed. The periods utilized for construction of the

satellite monthly climatologies were: (1) 1984 to 1990 for Gautier et al. data set, (2) 1985 to 1990 for both the Li et al. and Darnell et al. data sets, (3) July 1983 to June 1991 for the Bishop et al. data set, and (4) April 1985 to January 1989 for the Zhang et al. data set. In the case of the Zhang et al. data set, only the January, April, July, and October values were available. For this case, the intervening months (e.g., February, March) were interpolated from the available mean monthly values.

In addition to the monthly satellite retrievals, high-frequency retrievals based on a slightly revised version of the *Bishop et al.* [1997] technique (hereafter referred to as BR2+) were available for the period overlapping the Subduction experiment. The main revisions include using ISCCP DX instead of C1 data and treating ice and water clouds separately (James Bishop, personal communication, 1999). These data have a 0.5° spatial resolution and a temporal sampling of 3 hours. For comparisons to the buoy values, daily average time series were constructed using the pixel values nearest each buoy.

3. Clear-Sky Flux: Modeled Versus Observed

3.1. Observed Values

In order to compare the observed clear-sky flux values to model calculations, it is necessary to filter out cloudy periods from the buoy time series. The method used in this study follows, with some minor modifications, the satellite-based approach developed by *Waliser et al.* [1996] for deriving the clear-sky flux for the COARE IMET buoy [*Weller and Anderson,* 1996]. The cloud-filtering scheme utilizes the ISCCP DX data which has a temporal sampling of 3 hours and a spatial resolution of 30 km, although the data within any one grid cell comes from a single (subsampled) satellite pixel with a resolution of ~5 km. The DX quantities used for cloud screening include the cloud-detection flag and the visible reflectance from the grid cell nearest to the buoy locations. Using these parameters, the cloud screening is performed based on four screening criteria.

The first cloud screening criterion requires that the time of the (15-min average) buoy sample must fall within the 3-

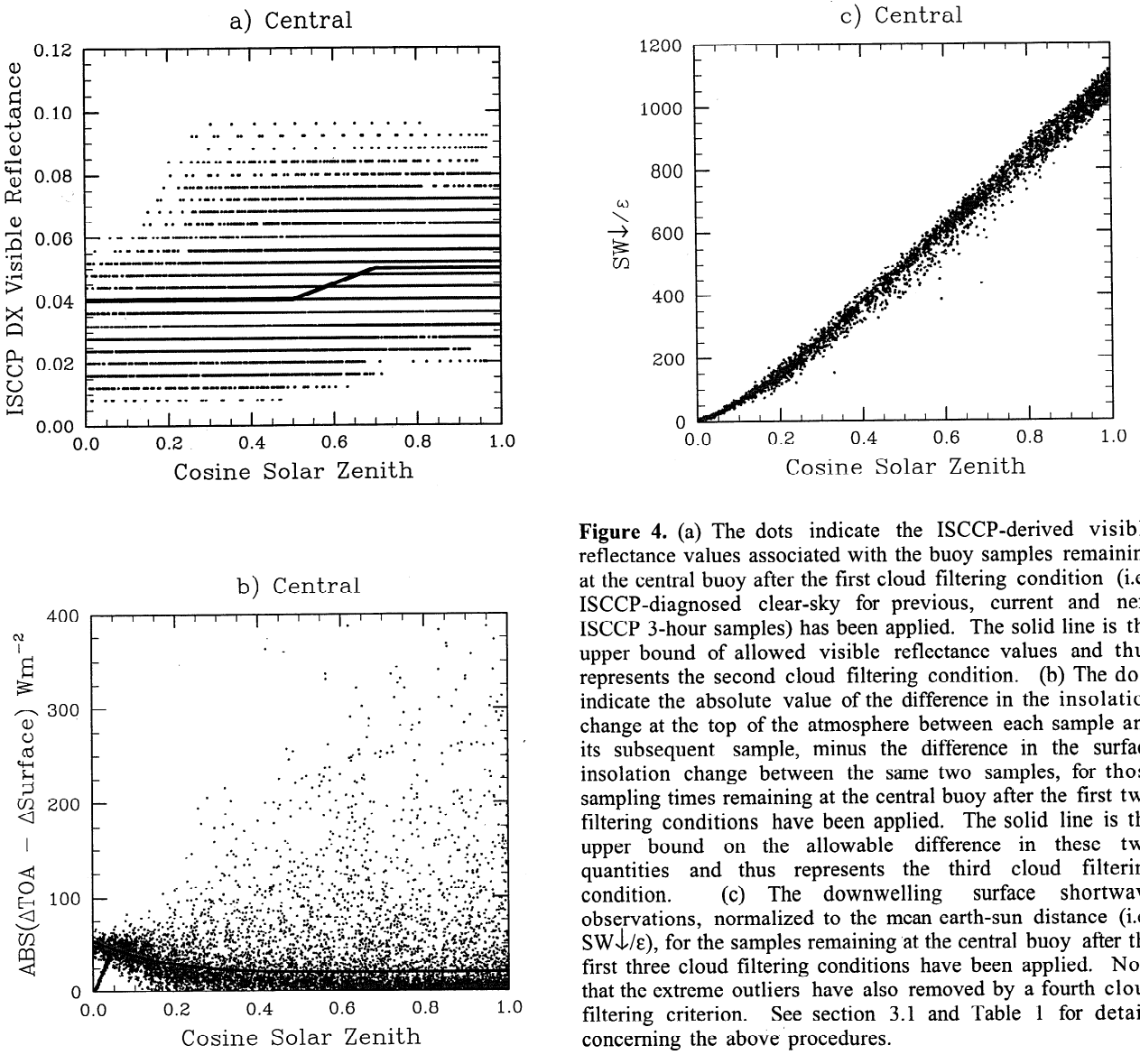

Figure 4. (a) The dots indicate the ISCCP-derived visible reflectance values associated with the buoy samples remaining at the central buoy after the first cloud filtering condition (i.e., ISCCP-diagnosed clear-sky for previous, current and next ISCCP 3-hour samples) has been applied. The solid line is the upper bound of allowed visible reflectance values and thus represents the second cloud filtering condition. (b) The dots indicate the absolute value of the difference in the insolation change at the top of the atmosphere between each sample and its subsequent sample, minus the difference in the surface insolation change between the same two samples, for those sampling times remaining at the central buoy after the first two filtering conditions have been applied. The solid line is the upper bound on the allowable difference in these two quantities and thus represents the third cloud filtering condition. (c) The downwelling surface shortwave observations, normalized to the mean earth-sun distance (i.e., $SW\downarrow/\varepsilon$), for the samples remaining at the central buoy after the first three cloud filtering conditions have been applied. Note that the extreme outliers have also removed by a fourth cloud filtering criterion. See section 3.1 and Table 1 for details concerning the above procedures.

hour time span of an ISCCP sample for which the cloud flag for the previous, current and subsequent ISCCP samples are all equal to zero. This step enforces clear-sky conditions in a large-scale sense over the buoy location. However, because the satellite footprint is much larger than the buoy radiometer's field of view and because the satellite sample is based on a single instantaneous pixel value representing a 3-hour time period, additional constraints need to be applied in order to filter out small-scale or thin clouds.

The second screening criterion lowers the allowable satellite-retrieved visible reflectance value for a sample to be considered clear-sky. For example, Figure 4a shows the reflectance values for the samples remaining at the central buoy after the above large-scale cloud filtering condition has been applied. In order to further reduce the cloud contamination, only samples with visible relfectance values below the thick line shown in Figure 4a are retained. The structure and levels of this limit were chosen to be as low as possible and still allow sufficient sampling at all values of $\cos(\theta_o)$, where θ_o represents the cosine of the solar zenith angle. (Below 0.04 for $\mu <= 0.5$, below 0.05 for $\mu >= 0.7$, below $[0.04 + (\mu - 0.5)\ 0.05]$ for μ in between 0.5 and 0.7, where $\mu=\cos(\theta_o)$.) Since the ocean is generally much less reflective than clouds, this criterion simply decreases the likelihood of contamination by isolated or thin clouds that are not screened out by the 3-hour sampling and large-scale footprint of the satellite values. The exact form of the specification applied was subjectively determined with the overall goal of simply removing a large fraction of the most reflective pixels and still retain roughly equivalent numbers of samples at all values of $\cos(\theta_o)$. While a number of variations of this criterion were examined, the quantitative form of the threshold had negligible impact on the final results.

The third screening criterion discards samples if the change in their insolation values with respect to the previous or subsequent values is greater than the expected change in the top of the atmosphere shortwave over that same time interval, plus some uncertainty. The idea here is that if the TOA value changes by a given amount between samples, then the surface value should change in a comparable way under clear-sky conditions. If the change at the surface deviates considerably from this behaviorm then it is likely to be influenced by the motion or evolution of nearby clouds. A similar criterion was developed and applied by *Bishop et al.* [1997]. Figure 4b shows, for those samples remaining at the central buoy after the first two conditions have been applied, the absolute value of the difference in the TOA insolation change between each sample and the subsequent sample, minus the difference in the surface insolation change between the same two samples. The solid line represents the upper bound on the allowable difference in these two quantities. (Threshold equals: $\{20 + 35\ [1-\cos(\theta_o)]^6\}$ W m^{-2}.) Again, the structure and level of this threshold was subjectively chosen to be as low as possible and still allow adequate and even sampling at all values of $\cos(\theta_o)$. As with the previous criterion, the final results are quite insensitive to the exact specification of the threshold. The subjectivity associated with the second and third criteria introduces some limitations with respect to their universal application to other locations. These limitations and their possible and the means to overcome them are discussed in the Summary and Discussion section.

Table 1 presents the results of the above three filtering procedures for each of the buoy locations. Table 1 shows that the available samples from each buoy are reduced by ~30% due to filtering criterion one (i.e., ISCCP DX cloud flags), by

Table 1. Cloud Filtering Criterion Applied to the Buoy-Measured Shortwave Values

Clear-Sky cloud Filtering Condition	Samples Removed	Samples Remaining	Percent Remaining
Northwest		19,951 *	51.17
Criterion 1, ISCCP DX cloud flags	13,617	6,334	16.25
Criterion 2, lower visible reflectance	2,285	4,049	10.39
Criterion 3, sample-to-sample change	1,987	2,062	5.29
Criterion 4, gross error check	3	2,059	10.32
Northeast		34,941 *	50.54
Criterion 1, ISCCP DX cloud flags	23,847	11,094	16.05
Criterion 2, lower visible reflectance	3,487	7,607	11.00
Criterion 3, sample-to-sample change	3,914	3,693	5.34
Criterion 4, gross error check	18	3,675	10.52
Central		34,934 *	50.38
Criterion 1, ISCCP DX cloud flags	21,306	13,628	19.65
Criterion 2, lower visible reflectance	5,667	7,961	11.48
Criterion 3, sample-to-sample change	4,225	3,736	5.39
Criterion 4, gross error check	6	3,730	10.68
Southwest		24,370 *	50.52
Criterion 1, ISCCP DX cloud flags	14,866	9,504	19.70
Criterion 2, lower visible reflectance	5,013	4,491	9.31
Criterion 3, sample-to-sample change	3,030	1,461	3.03
Criterion 4, gross error check	9	1,452	5.96
Southeast		29,292 *	51.02
Criterion 1, ISCCP DX cloud flags	17,993	11,299	19.68
Criterion 2, lower visible reflectance	6,373	4,926	8.58
Criterion 3, sample-to-sample change	3,188	1,738	3.03
Criterion 4, gross error check	20	1,718	5.87

* Initial number of samples take into account the removal of nighttime observations.

~5-10% due to filtering criterion two (i.e., lowering the allowed ISCCP DX reflectance values), and by ~5% due to filtering criterion three (i.e., limiting the sample-to-sample change). Note that the above percentages are associated with the total number of samples, daytime plus nighttime samples. Figure 4c shows the remaining insolation samples at the central buoy, normalized to the same Earth-Sun distance, versus $\cos(\theta_0)$. Note that the expected quasi-linear relationship between clear-sky downwelling shortwave and $\cos(\theta_0)$ only holds for $\cos(\theta_0)$ greater than ~0.2 [*Cess and Vulis,* 1989]. Figure 4c, and those for the other buoys (not shown), indicate that the above cloud screening procedures are very effective at screening out cloudy periods from the data. However, there is evidence of a few outliers in the remaining samples that suggest some remaining cloud-contaminated values. In order to filter these out, a regression of the normalized insolation values is made versus $\cos(\theta_0)$, and then any value that deviates from this regression by more than 125 W m^{-2} are also discarded. Table 1 shows that the number of samples filtered out due to this final filtering criterion is at most 20 samples. The final number of clear-sky insolation samples remaining for each buoy are also given in Table 1. These values range between about 1500 and 3700 and represents anywhere between 6 and 11% of the total daytime samples from each buoy.

3.2. Modeled Values

The modeled clear-sky flux values were computed using the single-column radiation model [*Briegleb,* 1992] from the National Center for Atmospheric Research's (NCAR) Community Climate Model (Version 3, hereafter CCM3 [*Kiehl et al.* 1996]). In these calculations, the atmosphere is divided into 17 atmospheric layers ranging from 10 to 1000 mbar (the same levels used in the NCEP/NCAR reanalysis [*Kalnay et al.,* 1996]). The total column water vapor is taken from colocated SSM/I retrievals. The mixing ratio in the lowest model layer is specified from the buoy observations, and the remaining water vapor is distributed upward through the model layers at the same constant mixing ratio value until no water vapor remains (i.e., a constant mixed layer). The sensitivity of the calculations to this assumption is discussed in section 3.3. The surface pressure is taken from the buoy observations and the ozone profile taken from a 12-month, zonally averaged, climatology [*Grose and Gille,* 1996]. Beginning with CCM3, a treatment of aerosols has been incorporated. The modeled aerosol effects are based on a prescribed sulphate aerosol which is nearly conservative in the visible range and modestly absorbing in the near infrared. In all model calculations performed in this study, the value of the aerosol optical depth is held fixed at 0.12 (the default value in the CCM3 single-column radiation code). Finally, the model clear-sky values described in the next section are based on computations using the time associated with the centers of the 15-min buoy averages.

3.3. Results

Figure 5 shows the agreement between the model-calculated and observed surface shortwave values for clear-

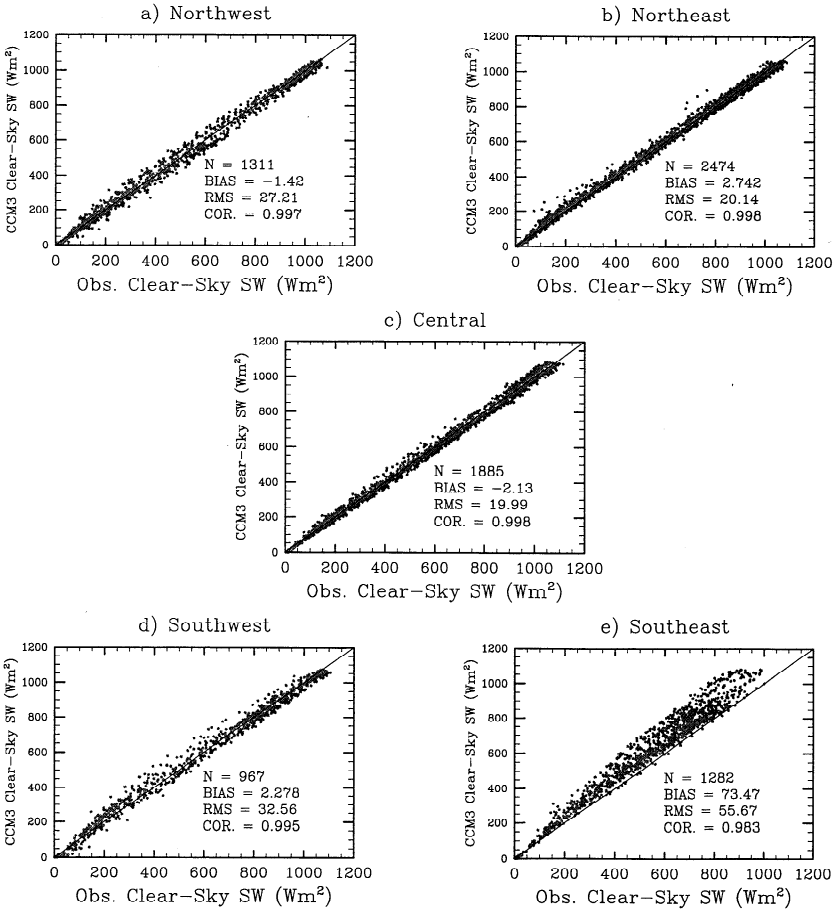

Figure 5. Scatterplots of observed (x axis) and modeled (y axis) clear-sky surface shortwave values at each buoy location. Note that the northwest, southwest, and southeast (northeast and central) buoys had toroid (discus) hulls.

sky periods for the five Subduction Experiment buoys. Note that the number of clear-sky samples available for comparisons (Table 1) has been reduced due to missing water vapor values and/or due to missing meteorological information (e.g., relative humidity, see section 2). Table 2 indicates the number of clear-sky samples that have been discarded due to missing auxiliary information needed for the model calculations. Note that these conditions are tested serially in the order given, thus the condition for the availability of buoy-measured meteorological data is only tested after the condition for availability of satellite water vapor. In general, the missing water vapor values reduce the number of available clear-sky samples by ~25-35% and missing meteorological information has a significant impact on the available samples only at the central mooring site where it reduces the number of clear-sky samples by ~20%. After accounting for this missing information, the number of points for comparison at each buoy ranges between about 700 and 1800 (see Table 2, third column and third row for each buoy). The plots for the northwest, northeast, central and southwest buoys show very good agreement with biases of only -0.3%, 0.5%, -0.4%, and 0.4%, respectively. Given that the mean value for each buoy's clear-sky time series is of the order of 500 W m^{-2}, this implies mean model versus observed biases of the order of 2-3 W m^{-2}. The associated root-mean-square (RMS) differences for these same four buoys range between about 20 and 35 W m^{-2}. These relatively small model-data differences for clear-sky surface shortwave values are consistent with those found by a number of other investigators [e.g., *Cess et al.,* 1996; *Conant et al.,* 1997; *Zender et al.,* 1997; *Jing and Cess,* 1998]. To make sure that these results are not highly model dependent, identical calculations were carried out with *Harshvardhan et al.* [1987] radiation scheme as implemented in the Navy Operational Global Atmospheric Prediction System (NOGAPS) GCM [*Hogan and Rosmond,* 1991]. In this case, available model values were net surface shortwave and so the buoy values were converted to the same quantity using an assumed albedo of 0.06 *[Payne,* 1972]. The magnitudes of the resulting model-data bias and RMS values were very similar.

The model-data comparison for the southeast buoy is quite different from the four discussed above, showing that the modeled downwelling shortwave is biased high relative to the observations by over 70 W m^{-2}. Further, the RMS difference is also significantly larger, having a value of 56 W m^{-2}. The sign of the bias for the southeast mooring, along with its larger amplitude, is somewhat expected given the mean monthly aerosol estimates shown in Figures 1 and 2. If this bias could be solely attributed to the enhanced atmospheric aerosols overlying this buoy, it would represent an aerosol forcing of 70 W m^{-2} on top of the background forcing already included in the model. (Examining differences between these results and a version of the model without aerosol effects showed that the background aerosol forcing, based on a fixed optical thickness of 0.12, is ~20-25W m^{-2} in this region.) However, the larger bias and RMS values for the southeast buoy may not be solely attributed to atmospheric aerosol but could also be due to aerosol buildup on the radiometer itself. At the time the buoy was retrieved, it was noted that the entire exposed portion of the buoy was covered with a reddish dust. Care was taken to try and preserve the dust on the radiometer in order to perform postdeployment calibrations with and without the dust on the sensor. While these two postcalibrations differed by only 1%, it is not known if all the dust residing on the instrument at the time of retrieval was

Table 2. Missing Ancillary Data for Buoy-Measured Clear-Sky Shortwave Samples

Missing Ancillary Data Type*	Samples Removed	Samples Remaining	Percent Remaining
Northwest		2,059 #	100.00
Satellite water vapor	748	1,311	63.67
Buoy meterological data	0	1,311	63.67
Satellite aerosol (AVHRR)	816	495	24.04
Satellite aerosol (TOMS)	1,062	249	12.09
Northeast		3,675 #	100.00
Satellite water vapor	1,201	2,474	67.32
Buoy meterological data	0	2,474	67.32
Satellite aerosol (AVHRR)	1,534	940	25.58
Satellite aerosol (TOMS)	1,976	498	13.55
Central		3,730 #	100.00
Satellite water vapor	1,151	2,579	69.14
Buoy meterological data	694	1,885	50.54
Satellite aerosol (AVHRR)	1,141	744	19.95
Satellite aerosol (TOMS)	1,641	244	6.54
Southwest		1,452 #	100.00
Satellite water vapor	371	1,081	74.45
Buoy meterological data	114	967	66.60
Satellite aerosol (AVHRR)	626	341	23.48
Satellite aerosol (TOMS)	719	248	17.08
Southeast		1,718 #	100.00
Satellite water vapor	423	1,295	75.38
Buoy meterological data	13	1,282	74.62
Satellite aerosol (AVHRR)	775	507	29.51
Satellite aerosol (TOMS)	889	393	22.88

* Only one of the aerosol products is considered at a time.

From Table 1, column 3, lower row of each buoy subsection.

still residing on the instrument during the laboratory calibration procedure. Moreover, it is not known how much variability there was in the amount of aerosol (i.e., dust) residing on the sensor over the course of the experiment. However, it is worth highlighting that the differences between the clear-sky model calculations and the upper envelope of the all-sky values for the southeast buoy shown in Figure 3 are typically smallest right after a deployment and then seem to grow with time. This suspect growth in model-data differences after buoy deployments, combined with: (1) the fact that there is virtually no other region over the world's oceans that contain higher aerosol deposition rates than that associated with the general location of the southeast buoy [*Prospero,* 1996]; (2) the rarity of strong precipitation events in this region that would assist in keeping the sensor free from aerosol build-up (Figs. 1-2); (3) the layer of dust found on the southeast mooring and sensor which was not found to any significant extent on the other moorings; and (4) the overall and significantly greater model-data bias for the southeast buoy, lead us to conclude that the quality of the shortwave observations from this buoy is too suspect to retain in subsequent aspects of this analysis.

Table 3 presents the results of the sensitivity tests associated with the computation of the clear-sky shortwave values for each of the four remaining buoys. In Table 3, the biases listed under "Base Case" are the mean relative biases between the modeled and observed values [i.e., 100(model-observed) /observed] for the computations described above and presented in Figure 5. The values in subsequent rows are the differences between the relative biases for the case listed and the base case. Thus the values listed below the base case provide a measure of the sensitivity to the given condition/perturbation. The first pair of tests illustrate the sensitivity of the clear-sky downwelling radiation calculation to a change in the surface albedo (factors of 0.8 and 1.2, respectively) which influences the radiation reflected up from the surface and then backscattered back down to the surface. In these cases, the ±20% perturbation in the surface albedo results in less than ±0.1% change in the model-observed bias (i.e., about ±0.5 W m^{-2}). The next pair of tests assess the uncertainty associated with the total column water vapor amount by adding ±10% to the observed value. In this case, the sensitivity is a little greater but still only results in about a ±0.5% change. The third pair of tests show the sensitivity of a ±10% change in column ozone. The sensitivity shown is about ±0.1% in all cases. The fourth pair of tests measures the impact of our assumption that all the column water vapor resides in a mixed-layer with a value determined from the buoy observations (See section 3b). The "shallow moist" ("deep dry") case, gives the change in the computation assuming that the surface value is 20% larger (smaller) and thus the same total amount of water vapor fits into a shallower (deeper) mixed layer. Note that this simplifying assumption also introduces only about a 0.5% change or less (i.e., about ±2.5 W m^{-2}).

In contrast to the four pairs of tests discussed above, the three pairs of sensitivity tests at the bottom of the table have significantly more impact. The first pair is due to a ±50% change in the specified aerosol optical thickness (a highly uncertain quantity). Here the differences are of the order of 1-2% or ~10 W m^{-2}. The second pair assesses the sensitivity to small amounts of cloudiness. The first test in the pair assumes scattered low-level clouds with cloud fraction 0.1 and a cloud liquid water path of 16 gm m^{-2}. The second test assumes a high-level cirrus cloud with cloud fraction 0.9 and liquid water path of 2 gm m^{-2}. In both these cases, the sensitivity is also ~2%. The last pair in the table tests the sensitivity of buoy tilt. In the "tilt away" case, the calculation is done with the buoy systematically tilted away from the Sun 1°. In the "tilt toward" case, the calculation is done with the buoy systematically tilted toward the Sun 1°. In these cases, the changes to the biases are about 2-3%, or ~10-15 W m^{-2}.

The higher bias values for the aerosol, cloud, and zenith angle tests indicate that these may be the more dominant sources of the RMS differences between the observed and calculated values shown in Figure 5. In the case of clouds, the source of error would be attributable to cases in which small-scale, isolated, or thin cirrus clouds were not completely screened out of the observations. In the case of aerosol, the errors are likely associated with synoptic, and possibly seasonal, aerosol variability that is not accounted for in the model calculations since the aerosol type and amount is fixed.

Table 3. Sensitivity Tests for Calculating Clear-Sky Downwelling Surface Shortwave

Base Case	Northwest	Northeast	Central	Southwest
Hull type	toroid	discus	discus	toroid
Number of samples *	1311	2474	1885	967
Number of unique days	127	236	197	160
Observed mean, W m^{-2}	457.1	510.7	511.4	544.0
RMS difference, W m^{-2}	27.2	20.1	20.0	32.6
Relative bias, %	-0.3	0.5	-0.4	0.4
Change in Percent Relative Bias Due to Given Perturbation (See Sections 3.2 and 3.3)				
Albedo(0.8)	0.0	-0.1	0.0	-0.1
Albedo(1.2)	0.1	0.1	0.1	0.0
Water vapor(0.9)	0.5	0.5	0.4	0.5
Water vapor(1.1)	-0.4	-0.5	-0.4	-0.4
Ozone(0.9)	0.2	0.1	0.1	0.1
Ozone(1.1)	-0.1	-0.1	-0.1	-0.1
Shallow-moist	-0.3	-0.4	-0.3	-0.3
Deep-dry	0.3	0.4	0.4	0.3
Aerosol(0.5)	1.7	1.6	1.6	1.5
Aerosol(1.5)	-1.6	-1.4	-1.5	-1.4
Scattered,low cloud	-1.8	-1.7	-1.8	-1.6
Thin, high cirrus	-2.2	-2.0	-2.1	-2.0
Tilt away	-2.8	-2.4	-2.6	-2.2
Tilt toward	2.8	2.5	2.6	2.3

* From Table 2, column 3, third row of each buoy subsection.

Errors in the zenith angle apply to the case of the buoy-observed fluxes due to the rocking motion of the buoys as well as any associated mean tilt induced by the prevailing mean currents.

Previous analytic [*Katsaros and DeVault,* 1986] and laboratory [*MacWhorter and Weller,* 1991] studies have shown that while time average errors (e.g., hourly or longer averages) due to buoy rocking motion tend to be small, errors due to mean tilts can be significant when tilts toward or away from the sun change the apparent zenith angle. These results suggest that buoy rocking motion due to ocean swell and buoy tilt due to ocean current variability are likely playing a nontrivial role in the RMS differences between modeled versus observed values. In fact, it is worth noting that the RMS differences are ~50% higher at the sites with toroid buoys (northwest and southwest) compared to the sites with discus buoys (northeast and central). This might suggest that the toroid buoys are less stable observational platforms under the conditions of the Subduction Experiment. However, without further information on the actual buoy tilt as a function of time, it is hard to determine if this is indeed the case. It is worth pointing out that the effects from tilting will be significantly reduced under cloudy skies when the radiation is more diffuse, and in fact, there is some evidence of this in the all-sky comparisons presented in section 5.

The above discussion suggests that most of our model-data differences are likely due to contamination by clouds, influences of unaccounted for aerosol variability, buoy tilt and possibly errors in water vapor retrievals. Given we have observations of water vapor and an estimate of aerosol amount, we can use these to determine if there are any systematic errors in the model-data differences associated with these quantities. Figure 6 shows the relative errors, in terms of percentage, between the modeled and observed values for the northwest, northeast, central and southwest buoys versus water vapor. Each bin has the same number of values in the average. This number is given by the total number of values for all bins combined (see third sub-row for each buoy in Table 2) divided by five. These plots indicate that there is no consistent systematic error introduced into the model calculation due to variability of water vapor. In other words, the model seems to correctly account for the effects of water vapor in the clear-sky atmosphere.

To examine the relationship between model-data errors and aerosol variability, daily aerosol retrievals based on two different algorithms were obtained (see section 2.2). The first is based on AVHRR data and the agorithm of *Stowe et al.* [1997], while the second is based on TOMS and the algorithm of *Herman et al.* [1997]. Owing to the missing data in each of the these aerosol data sets, it was necessary to reconstruct the comparisons shown in Figure 5 and Table 3 using only the clear-sky buoy observations which had an aerosol measurement for that day. The reduction in the number of clear-sky samples due to missing aerosol values is shown in Table 2 (fourth and fifth sub-row for each buoy). Typically, this reduction amounted to ~40-50% of the original clear-sky samples, leaving anywhere from 341 to 940 (244 to 498) clear-sky samples with AVHRR (TOMS) aerosol retrievals. The number of samples remaining after accounting for the missing AVHRR and TOMS observations are repeated in the first and fifth rows, respectively, of Table 4. This table also shows the number of (unique) days that these (15-min) buoy samples actually came from. In addition, Table 4 shows the average buoy-observed insolation values for these remaining samples and the mean relative biases between the modeled and observed values for this subset of samples, assuming the "base case" model assumptions described above. Note that the relative bias errors are very similar to the cases of the complete set of clear-sky measurements given in the sixth row of Table 3.

Figure 7 shows the relative errors, in terms of percentage, between the modeled and observed values for the northwest,

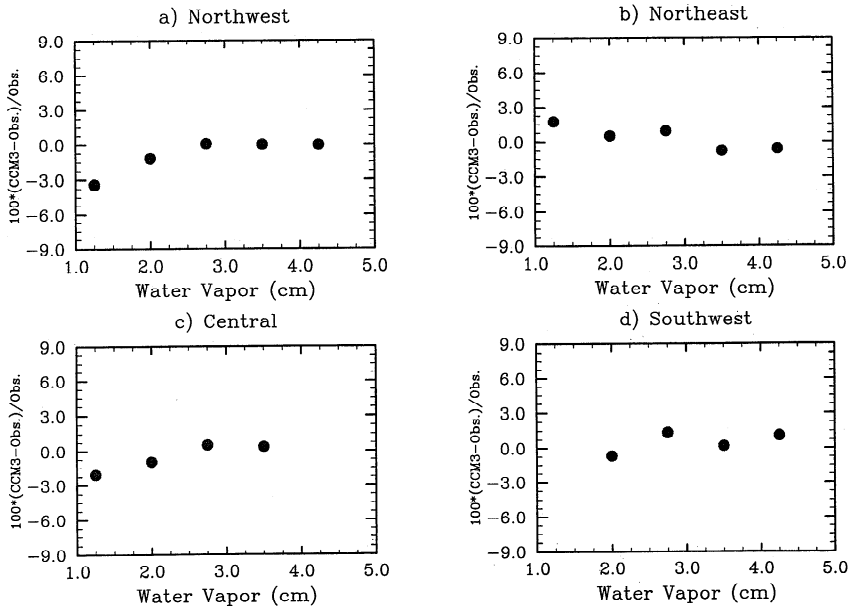

Figure 6. Relative errors, in terms of percentage, between the modeled and observed clear-sky surface shortwave values for the (a) northwest, (b) northeast, (c) central, and (d) southwest buoys versus columnar water vapor amount. The *x* axis bin sizes are every 0.75 cm water vapor.

Table 4. Relative Biases Using Only the Samples When Aerosol Values Available

	Northwest	Northeast*	Central	Southwest
AVHRR-Aerosol				
Number of samples	495	940	744	341
Number of unique days	42	75	76	46
Observed mean, W m^{-2}	527.2	547.1	527.4	525.5
Relative bias, %^	0.4	0.3	0.0	-0.1
TOMS-Acrosol				
Number of samples &	249	498	244	248
Number of unique days	26	51	37	58
Observed mean, W m^{-2}	509.6	554.6	605.7	503.7
Relative bias, %^	0.0	0.0	0.1	1.5
Number of Common Samples	99	255	85	89
Number of Common Days	12	20 (19)	11	15
Correlation on Common Days	-0.05	0.49 (0.29)	0.51	0.40

Modeled aerosol value held constant at base case value (see Sections 3.2 and 3.3).
* Values in parentheses are the values when the large outlier is removed (see Fig. 8).
+ From Table 2, column 3, fourth row of each buoy subsection.
& From Table 2, column 3, fifth row of each buoy subsection.
^ Here, 100(model - observed)/observed.

northeast, central and southwest buoys versus AVHRR aerosol optical thickness for the clear-sky samples having observations with this aerosol retrieval. The results appear to be mixed. The model-data differences for the northwest and northeast buoys show no obvious influence from aerosol, at least not the expected increase in difference with aerosol amount, while those for the central and southwest buoy do show such an increase. The relationship for the latter two is somewhat similar to that found by *Jing and Cess* [1998] for three coastal stations in Canada. However, it is not obvious why the two northerly stations exhibit a different behavior. To help determine the reliability of these results and help with their interpretation, similar plots were constructed with clear-sky samples that had TOMS aerosol retrievals (not shown). Interestingly, the model-data differences versus the TOMS aerosol show no clear, systematic increase with increasing aerosol amount at any of the four buoys.

The above results concerning the influence of aerosol raises a number questions. Given the model uses a fixed aerosol amount, why do the differences between the modeled and observed values increase with the observed aerosol amount only for the central and southwest buoys, and then only for the AVHRR product? Why don't these model-data differences increase with increasing aerosol for the northwest and northeast buoys for either of the aerosol products? Determining definitive answers to these questions turns out to be extremely difficult given the available data. To begin with, it is important to remember that the two aerosol retrievals tend to highlight different types of aerosols. The TOMS retrieval is best at detecting aerosols such as smoke plumes, dust, and volcanic ash, all of which have an absorbing signature in the UV, and poor at detecting for example (nonabsorbing) sulphate aerosols. On the other hand, the AVHRR retrieval is best at detecting strongly scattering aerosols, which include sulphate aerosols as well as some absorbing aerosols that still exhibit significant scatter (e.g., dust). In fact, it is worth pointing out that Stowe et al. specifically indicate that of all the aerosol types over the

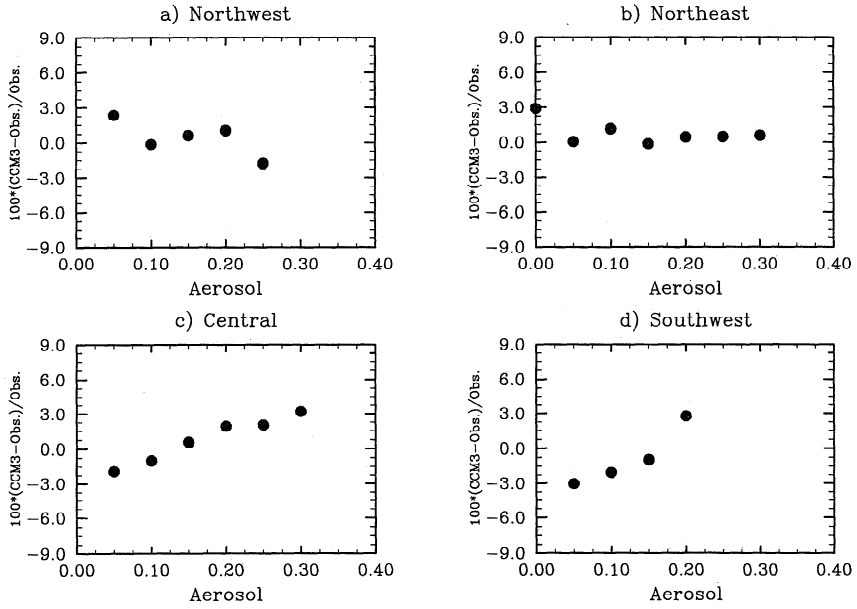

Figure 7. Same as Figure 6, except for aerosol optical thickness from AHVRR [*Stowe et al.*, 1997], and only for the samples that had available aerosol retrievals. The *x* axis bin sizes are every 0.05 optical thickness. See section 3.3.

ocean, mineral dust (i.e., the type of dust coming off northern Africa) is the least similar to their assumed aerosol model and therefore is the most uncertain in terms of their estimates. Along with the above limitations regarding the type(s) of aerosols each retrieval is inherently insensitive to, there are additional limitations associated with each of the retrieval techniques. For example, Herman et al. indicate that their method tends to only detect absorbing aerosols above 1 km, and therefore those in the boundary layer cannot be readily detected. Likewise, there are still significant uncertainties in the AVHRR retrievals due to its single-channel approach and the use of a single, fixed value of water vapor and ozone amount for all locations.

The characteristics and shortcomings of the AVHRR and TOMS aerosol retrievals discussed above imply that neither product alone is able to represent the influence on the surface shortwave from the different types and amounts of aerosol present in the atmosphere over the Subduction area. Adding to these measurement difficulties, is the fact that the sources of aerosol over the area of the Subduction Experiment are highly complex [see *Husar et al.,* 1997]. This region contains a significant amount of mineral dust transported westward from northern Africa, sulphate and smoke aerosols from southern Europe, ocean-borne aerosols from the local surroundings, as well as outfall from biomass burning to the south. In addition, the Subduction Experiment started the same month as the Mount Pinatubo volcanic eruption. This event injected considerable amounts of aerosol (H_2SO_4-H_20 and volcanic ash) into the tropical stratosphere. *Russell et al.* [1996] describe the global and microscale evolution of these aerosols which turns out to be considerable over the subsequent 12-18 months.

The results and discussion above suggests that the "aerosol" influence on the surface shortwave at the Subduction site may be anything but simple. For example, Figure 8 shows the relationships between the AVHRR and TOMS aerosol retrievals for those cases when both were available. The circles indicate the values of the daily aerosol retrievals for the overlapping cases (see next to last row in Table 4). The size of the circle indicates how many clear-sky shortwave (15-min) samples were associated with each daily value. Note that the correlations (last row in Table 4) between the two products are fairly poor, even negative for the case of the northwest buoy. The correlation for the northeast buoy is modest, ~0.5, however, most of this agreement comes from a large outlier which when removed lowers the correlation to 0.29. These relations show that even though the AVHRR aerosol value may be low, it is not necessarily the case for the TOMS aerosol. Such circumstances could lead to the ambiguous results regarding the plots of model-data differences versus aerosol amount discussed above. The relations for the central and southwest buoys have correlations of 0.5 and 0.4, respectively. In these cases, there is a tendency for a large range of AVHRR aerosol values with the TOMS values staying relatively uniform. This feature might have allowed the expected relationship between model-data difference and AVHRR aerosol amount to be more readily exhibited for these two buoys (Figure 7). In short, given the complex aerosol environment associated with the region of the Subduction Experiment, it was found that the available observations were inadequate (due to either insufficient sampling or measurements with large error characteristics) to derive a robust relation between aerosol amount and its affect on the surface shortwave.

4. Shortwave Cloud Forcing

The overall agreement illustrated in the previous section between observed and modeled clear-sky surface shortwave suggests that the model calculations provide a sound way to determine the clear-sky component of the surface shortwave insolation. From this information, along with the observed (all-sky) value, time series of surface shortwave cloud forcing can be derived. Following the methods used for the "base case" calculations of clear-sky shortwave, we have calculated clear-sky surface shortwave values for the northwest,

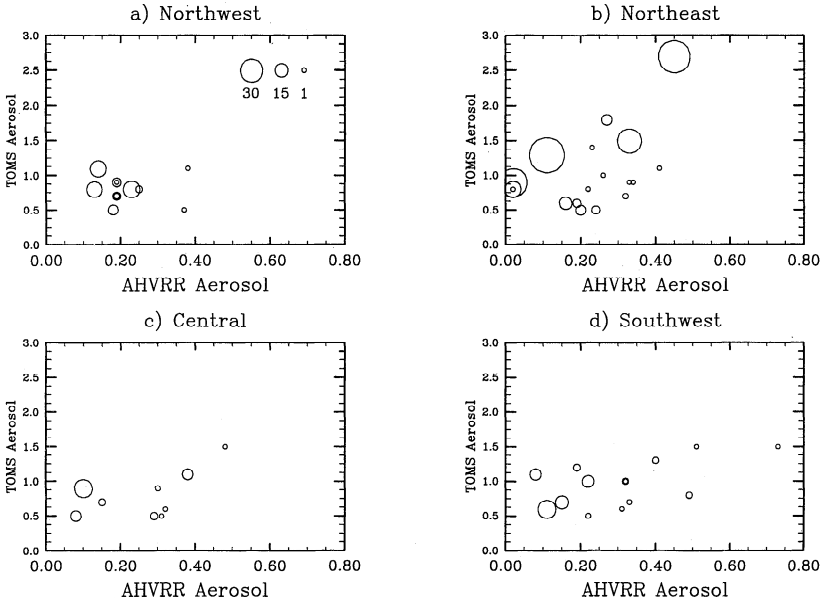

Figure 8. Scatterplots of AVHRR and TOMS aerosol retrievals for those samples/days when both were available. The circles indicate the values of the daily aerosol retrievals for the overlapping cases. The size of the circle indicates how many clear-sky shortwave (15-min) samples were associated with the given daily value See last subsection in Table 4.

Table 5. Missing Ancillary Data for Buoy-Measured All-Sky Shortwave Samples

Missing Data Type	Samples Removed	Samples Remaining	Percent Remaining
Northwest		19,948	100.00
Satellite water vapor	7,226	12,722	63.78
Buoy meterological data	0	12,722	63.78
Northeast		34,941	100.00
Satellite water vapor	12,313	22,628	64.76
Buoy meterological data	0	22,628	64.76
Central		34,931	100.00
Satellite water vapor	11,867	23,064	66.03
Buoy meterological data	5,071	17,993	51.51
Southwest		24,370	100.00
Satellite water vapor	6,323	18,047	74.05
Buoy meterological data	2,735	15,312	62.83

Removed and remaining samples only applies to daytime samples.

northeast, central and southwest buoys for each data sample that has the required ancillary data (e.g., water vapor, surface pressure, etc.). Table 5 shows the total number of daytime shortwave samples at each buoy, the reduction of available samples from missing water vapor and near-surface meteorological data. The missing water vapor data reduces the available samples by between 26 and 36%. These missing samples are evenly distributed in time throughout the two year period and are associated with the DMSP polar-orbiting satellite and SSM/I sensor which do not provide complete tropical coverage in a single day. Missing meteorological data only effects the central and southwest buoys. The missing meteorological data for the central buoy overlaps with ~15% of the remaining shortwave observations (i.e., after removing samples due to missing water vapor) and is composed of missing surface relative humidity observations between May and October 1992. The missing meteorological data for the southwest buoy overlaps with about 11% of the remaining shortwave observations and is composed of missing surface pressure observations starting in March 1992, ~2 months prior to the beginning of the second gap in the shortwave observations. Daily averaged values of these clear-sky time series are plotted in Figure 3. As expected, these values appear to correspond closely to the upper envelope of the all-sky values [cf. *Bishop et al.* 1997]

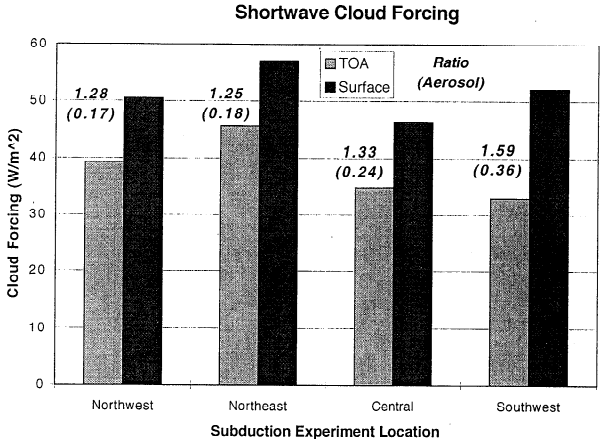

Figure 9. Surface (dark gray) and top of the atmosphere (TOA; light gray) mean shortwave cloud forcing values for the northwest, northeast, central, and southwest buoy locations. Surface values are derived from the all-sky buoy observations and modeled clear-sky values. TOA values are derived from a weighted mean of ERBE climatology, where the weighting is based on the data periods available from the buoy (See Figure 3). See section 4. Top number listed for each buoy is the ratio between the surface and TOA cloud forcing values. Bottom number is the mean aerosol optical thickness over the Subduction Experiment period.

The time series of buoy observed (all-sky) shortwave and the model calculated values of clear-sky shortwave are combined to form time series of surface shortwave cloud forcing. Mean values of this quantity are 50, 57, 46, and 52 W m^{-2} for the northwest, northeast, central and southwest buoys, respectively; these values are shown in Figure 9, which also shows the associated top of the atmosphere (TOA) shortwave cloud forcing values. These data are weighted means of 12-month climatological values derived from ERBE. The weighting is based on the calendar-year sampling of the buoy data. For example, the northeast buoy provides a near-continuous 2-year period (Figure 3), and thus the ERBE TOA value is nearly identical to just the long-term annual mean value at that same location. The central buoy, however, contains missing data during May to October 1992 due to the missing relative humidity, so the ERBE average contains only half the contribution from these months. Note that the interannual standard deviations of the annual mean ERBE values over the buoys for the 1985-1989 period is relatively small (~3-4.5 W m^{-2}; N=5), and thus the ERBE climatology is likely to be a good estimate of TOA cloud forcing for the period of the Subduction Experiment. To obtain some assurance of this, mean values of outgoing longwave radiation (OLR) [*Gruber and Krueger,* 1984] for the Subduction and ERBE periods were computed and compared. It was found that the mean OLR values from these two periods differed by ~4 W m^{-2} at the central buoy, by ~3 W m^{-2} at the two Southern buoys, and by less than 0.5 W m^{-2} at the two northern buoys.

The comparisons between the TOA and surface "mean" values shows that the surface values are always at least 25% larger than the TOA values, with surface to TOA shortwave cloud ratios ranging between 1.25 and 1.59. Assuming the errors in these ratios come mostly from the use of non-contemporaneous ERBE values, an estimate of error can be obtained by using the interannual standard deviations as a measure of their uncertainty. This widens the above range of ratios to lie between 1.17 and 1.84. Figure 9 lists the ratio for each buoy along with the mean aerosol amount over the

course of the experiment. There is a weak but positive relationship between the size of this ratio and the aerosol amount and thus the relatively large value for the southwest buoy (1.59) could be attributed to the larger amounts of aerosol over the southwest buoy compared to the other three buoys. In this context, the influence of these aerosols would be masked as cloud forcing rather than be properly and separately accounted for as aerosol forcing. This affect aside, these surface to TOA cloud forcing ratios, particularly those from the more pristine areas, agree with those in previous studies by *Ramanathan et al.* [1995], *Cess et al.* [1995], *Waliser et al.* [1996], *Cess et al.* [1996], and *Zender et al.* [1997]. These results add further support to the suggestion that observed clouds absorb more shortwave radiation than clouds modeled in a typical atmospheric general circulation model, the latter of which are known to have surface to TOA cloud forcing ratios of ~1.1 [e.g. *Cess et al.,* 1996].

5. Surface Insolation Comparisons

The long, continuous records of surface insolation from the Subduction Experiment provide the opportunity to validate bulk parameterizations and satellite retrievals of surface shortwave over the open ocean where radiometer observations are extremely rare. The data sets obtained for this comparison are discussed in section 2.2. Since the data sets that are based on bulk parameterizations using ship reports of cloudiness are only given in terms of climatological values and since most of the available satellite-derived data sets do not overlap the period of the buoy observations, the primary basis for comparison will be long-term mean values. Using the 12-month annual cycles computed for each data set, weighted long-term mean values were computed at each buoy location using only the periods of the calendar year when data was available in the associated buoy record (see Figure 3 and discussion of annual cycle weighting in previous section). Figure 10 shows the results of the comparisons between the two-year mean buoy values and the long-term means derived from satellites and bulk methods. For the ship-based comparisons, the agreement is mixed. The EK values for all the buoys are low relative to the buoy-observed values but still generally within ~5%. The Oberhuber values are significantly lower than the buoy-observed values. The relative bias is of the order of 20%. The difference in biases between the EK values and those from Oberhuber may stem from the tuning Oberhuber applied to his derived heat fluxes based on considerations of the meridional net surface heat flux profile. The tuning applied to the shortwave values was a multiplication factor of 0.9. This would account for at least 10% of the difference between the Oberhuber and EK ship-based values. The remaining part of the discrepancy is likely due to the difference in cloudiness correction factors used in deriving the insolation; EK used the correction of *Berliand* [1960] and Oberhuber used the correction of *Reed* [1977]. At least in the present context, it appears that the former may be more accurate for the types of cloud conditions that exist in the Subduction region.

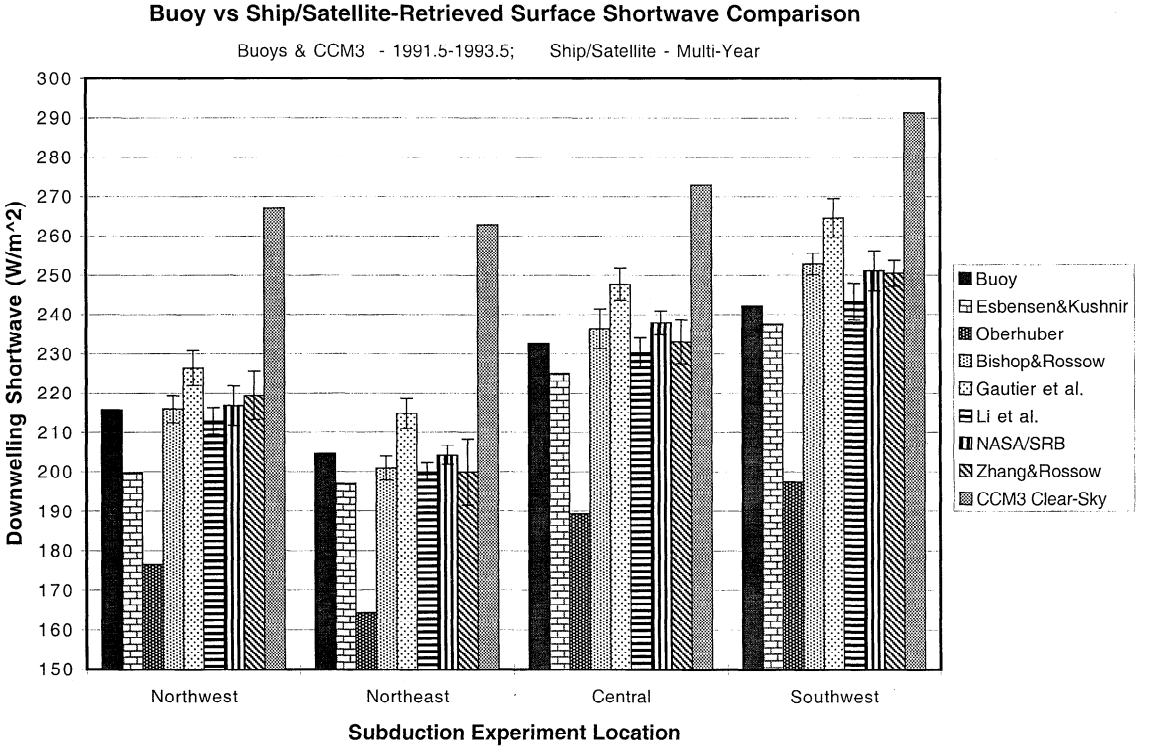

Figure 10. Comparison of mean downwelling surface shortwave values at the northwest, northeast, central and southwest buoy locations from the buoy observations, two ship-based climatologies, and five satellite-derived products. In the case of the satellite values, the error bars represent interannual standard deviations. The means for the buoys are for all the available all-sky observations, while the means for the ship- and satellite-derived values are weighted averages of the climatology based on the sampling of the buoys. Note, however, that the means for the clear-sky values are based only on periods when a clear-sky calculation was possible (i.e., no missing ancillary data; see Figure 3 and Table 5) and thus is made up of a subset of the samples used for the all-sky means. See section 5.

In the case of the satellite retrievals, most of the retrievals are within a few percent of the buoy observations. There is a tendency for the satellite retrievals to be biased high over the southwest buoy and this could possibly be attributed to the slightly higher aerosol amounts over this location relative to the other three. The high and low outliers in this group of satellite retrievals are Gautier et al. and Li et al., respectively. The data set from the former has values that are on average ~15 W m^{-2} higher than the average of the four buoy values, while the data set from the latter has values that are typically ~2 W m^{-2} lower than the buoy values. Most others show an average bias error of ~2-4 W m^{-2} higher than the average of the four buoy values. This range of bias between satellite and buoy values is similar to that found by *Bishop et al.* [1997] when comparing their retrieval to the MLML and Biowatt data.

Contemporaneous comparisons using daily average buoy and BR2+ satellite values are shown in Figure 11. These scatterplots only present values that are composed of a complete set of samples for the daily average (i.e., 96 15-min buoy samples and 8 3-hour ISCCP samples). In terms of the biases, the agreement is roughly equivalent to the agreement observed in the long-term mean comparisons above. Again at the southwest buoy, the satellite values are biased relatively higher than at the other three buoys, the latter of which are biased high relative to the buoy values by ~4 W m^{-2} or less. The RMS differences range between about 25 and 30 W m^{-2}. Interestingly, the noticeable differences in RMS values found between the toroid (northwest and southwest) and discus (northeast and central) buoys for the clear-sky comparisons (Figure 5) are not apparent in these all-sky comparisons. However, this feature is still consistent with the notion that the toroid buoys may be subject to more rocking and/or mean tilt, since the impact of such motion would have a significantly reduced impact in cloudy conditions when the source of radiation is significantly more diffuse. Note that very little of the disagreement in the biases or RMS differences can be attributed to the clear-sky model, since the observed clear-sky values compared quite well to the CCM3 values, which in turn compare very well to the clear-sky BR2+ values (not shown; biases ~1 W m^{-2}; RMS differences ~4 W m^{-2}). It is likely that most of the RMS difference in these daily average comparisons stems from the contrasts in spatial and temporal sampling between the two types of measurements.

6. Summary and Discussion

The goal of this study was to analyze and exploit the surface shortwave observations obtained from Subduction Experiment. This experiment consisted of five buoys deployed over a 2-year period from June 1991 to June 1993 in the subtropical north Atlantic Ocean off the west coast of Africa. Such long-running time series of surface shortwave flux over the open ocean are extremely rare and in fact unprecedented at the time the experiment had been completed. In this study, the data were utilized to address three questions. The first question involves the recent debate concerning clear-sky shortwave absorption and how well this quantity is predicted by theoretical radiative transfer models. Robust methods were used to isolate only the clear-sky buoy-measured shortwave observations so that they could be directly compared to values derived using a single-column version of the NCAR CCM3 radiation code. Surface meteorological information, climatological ozone amounts, and SSM/I-derived water vapor amounts were used as input to the model calculations. The results showed that the model-derived values agreed with the observations to within 0.5% mean relative error for four of the five buoys, with mean RMS differences of ~20-30 W m^{-2}.

Data from the buoy located at the southeast edge of the experiment, nearest the west African coast, was discounted early in the analysis due to the possibility that the radiometer

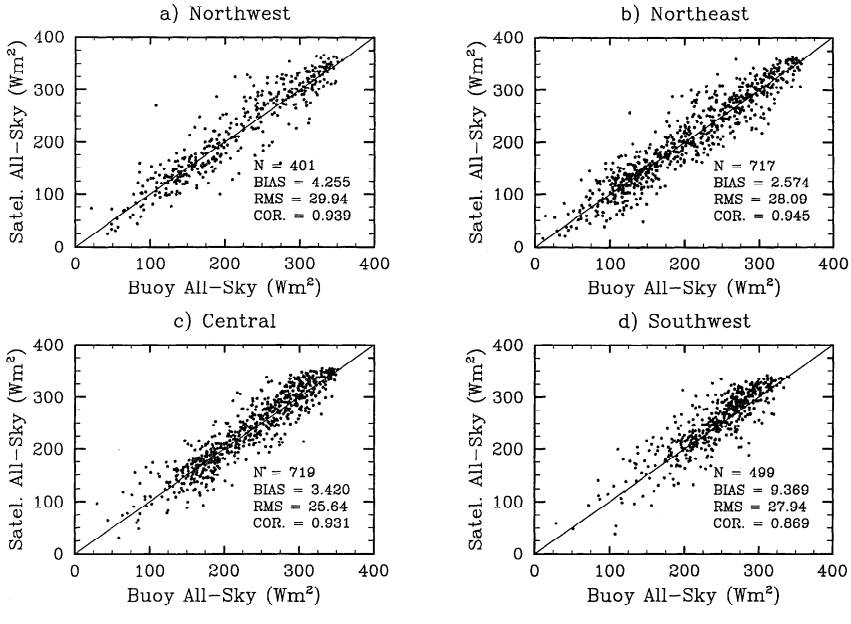

Figure 11. Contemporaneous comparisons between daily average buoy and satellite values of all-sky downwelling surface shortwave flux for the (a) northwest, (b) northeast, (c) central, and (d) southwest buoys. The satellite values are derived from a slightly revised version of *Bishop et al.* [1997] (see section 2.2). These scatter plots only present values that are composed of a complete set of samples for the daily average (i.e., 96 15-min buoy samples and 8 3-hour ISCCP samples).

was covered to varying degrees by atmospheric aerosol (i.e., Saharan dust) settling out of the atmosphere (see section 3.3). On the remaining four buoys, additional analysis was performed on the model-data differences with respect to AVHRR-derived and TOMS-derived aerosol amount to try and determine if there a systematic relationship between model-data agreement and observed aerosol amount. This part of the analysis led to inconclusive results due to the combination of a very complex aerosol environment [e.g., *Husar et al.,* 1997], insufficient clear-sky sampling and aerosol measurements with large error characteristics (see section 3.3). A similar analysis was performed on the relationship between model-data differences and column water vapor amount. The results of this analysis showed no systematic relationship with respect to column water vapor amount (e.g., the "errors" didn't increase with increasing column water vapor), and thus the absorption due to water vapor in particular appears to be well modeled. Additional sensitivity tests were performed on the numerical calculations and associated inputs that show the most likely source of the RMS differences are due to the unaccounted for aerosol variability, buoy tilting and possibly shortcomings in the cloud screening procedures. In fact, there was some evidence to suggest that the sensors mounted on discus buoys might have provided a more stable platform for measuring shortwave radiation than those mounted on toroid buoys. Overall, the very good agreement between the model-derived and observed clear-sky shortwave values for these four, 2-year records helps to further confirm that our theoretical radiative transfer models are properly accounting for shortwave energy in the clear-sky atmosphere.

The second question addressed by the analysis concerns the absorption of shortwave radiation by clouds. As stated in the introduction, there has been considerable debate regarding the representation of shortwave absorption by clouds in radiative transfer models. Typical GCMs exhibit a surface to TOA shortwave cloud forcing ratio of ~1.1, while a number of observational studies have found that this ratio to be larger, of the order of 1.2-1.5 (see introduction). Given the good agreement between the modeled and observed clear-sky values described above, the model was then used to derived clear-sky surface flux values for all the buoy samples that had the necessary ancillary data available (e.g., water vapor, surface pressure, etc.). The observed series and model-derived clear-sky series were combined to compute the surface shortwave cloud forcing. The mean of these series were combined with the mean shortwave cloud forcing values at the TOA from ERBE to determine the surface to TOA cloud forcing ratio. The values obtained for this ratio was 1.28, 1.25, 1.33, and 1.59. The first three values are from buoys located in relatively pristine air, while the latter, and largest, of the values was obtained from a buoy in relatively close proximity to the Saharan dust plume. The aerosol associated with this plume is known to have absorbing characteristics, and thus it is likely that this relatively high aerosol content is responsible for the relatively high value in this ratio. In any case, these values, along with the above agreement found between modeled and observed clear-sky surface shortwave support the suggestion that the current GCM radiation parameterizations are not properly accounting for the amount of shortwave energy absorbed by the cloudy atmosphere.

The third question addressed by the analysis concerns the accuracy of ship- and satellite-based retrievals of surface shortwave flux. Mean values of the shortwave flux time series were compared to mean values from the *Oberhuber* [1988] and *Esbensen and Kushnir* [EK; 1981] ship-based climatologies as well as to the satellite-derived products of *Gautier et al.* [1980], *Li et al.* [1993a], *Bishop et al.* [1997], *Zhang et al.* [1995] and *Darnell et al.* [1992]. The comparisons show that between the two ship-based climatologies, the Oberhuber data set underestimates the mean surface shortwave flux by ~20% (~40 W m^{-2}), while the EK data set underestimates the flux by ~4% (~8 W m^{-2}). The satellite products in general show better and more consistent agreement, with biases ranging from about -1 to 6%. Therefore, in the Subduction Experiment region, and thus likely in most subtropical ocean regions, satellite-derived surface shortwave fluxes appear to exhibit fairly accurate long-term mean values. In addition, comparisons to contemporaneous daily average values from a slightly improved version of the *Bishop et al.* [1997] scheme showed fairly good agreement, with biases of the order of 3-9 W m^{-2} and RMS differences of ~25-30 W m^{-2}.

Finally, we would like to comment on the implications of the above results for buoy-measured open-ocean shortwave flux. The results concerning the agreement between modeled and observed values of clear-sky shortwave do not come as a significant surprise given that a number of investigators have shown similar results using complimentary data sets (see introduction). While most of these previous studies used data that were more limited in time or space, the operating environment of the instrument was significantly less stressful and the maintenance of the instrument was most likely more routine and frequent. The operating environment and maintenance limitations associated with ocean buoys, along with the tilts they experience due to currents and ocean swell, have led to concerns about their ability to robustly measure or monitor open-ocean shortwave fluxes. The data, and associated instruments and moorings, used in this study indicate that moored buoys do indeed show great promise for providing long-term climate monitoring of surface radiation as well as validation data for satellite studies such as the Clouds and the Earth's Radiant Energy System (CERES) program [*Wielicki et al.,* 1996]. Moreover, the techniques demonstrated here for constructing model-derived shortwave values could be applied in a real-time diagnostic mode to ensure that the radiometer is still in proper working condition. For example, real-time cloud data could be used to detect cloud-free periods. For these periods, the satellite-relayed buoy observations (i.e., shortwave, surface pressure and humidity, etc.) could be combined with real-time satellite-derived water vapor and even ozone data to compute the clear-sky surface flux value. These modeled clear-sky flux values could be routinely compared to the observed values during these clear-sky periods to assess the operating condition of the radiometer and help assess the maintenance priority of a given mooring.

In order to apply the cloud filtering techniques developed in this study more universally, the thresholds associated with criteria two and three (see section 3.1) need to be formulated more objectively. This is especially true of criterion two, which screens clouds based on satellite reflectance values, which in turn are dependent on the satellite and solar zenith angles at the buoy location. One straightforward approach which closely follows, in principle, the formulation developed in this study, is to just remove a specified fraction (e.g., 50%) of samples at each $\cos(\theta_0)$ that

have the highest reflectance. This could easily be applied uniformly to any location and lead to the desired effect, i.e., remove the samples associated with the highest reflectance values which would tend to be the samples most likely to be contaminated by clouds. Further, such a formulation would uniformly filter all values of $\cos(\theta_0)$ and still leave clear-sky samples at each $\cos(\theta_0)$. The threshold for the third criteria could be administered in a similar manner in order to remove a given fraction of samples at each $\cos(\theta_0)$ that are associated with the largest sample-to-sample change in insolation. We are presently examining the efficacy of these modifications in our present research which involves employing similar methods to assess the overall quality and utility of buoys under operating conditions from a number of research experiments (e.g., FASINEX, MLML) and operational deployments (e.g., TOGA TAO) that include surface shortwave observations.

Acknowledgments. Support for this study was provided by the Radiation Science Program of the National Aeronautics and Space Administration under grant NAG-1-2065 (DW), the Marine Meteorology Program of the Office of Naval Research under grants N00014-97-10527 (DW) and N00014-90-J1490 (RW). This work was additionally supported by the Department of Energy through grants DEFG0285ER60314 and DEFG0290ER61063 to the State University of New York at Stony Brook (RC). The authors would like to thank Mike McPhaden (PMEL) and Bruce Wielicki (NASA) for their support in helping to obtain funding for this project. The moored array was deployed and maintained in collaboration with Russ Davis (Scripps Institution of Oceanography). We would like to thank Jeff Kiehl (NCAR), Minghua Zhang (SUNY), and Joe Prospero (U. Miami) for providing a number of useful comments regarding the analysis and presentation. We would like to thank Bruce Briegleb (NCAR) and Tim Hogan (NRL) for providing us with the CCM3 and NOGAPS single-column radiation model, respectively. We would also like to thank Pete Peterson (University of California, Santa Barbara) for providing the time series of SSM/I precipitable water, Larry Stowe and Jay Herman for providing aerosol data along with a number of helpful comments and clarifications, and Catherine Gautier, Zhanqing Li, Yuanchong Zhang, and James Bishop for providing their shortwave data sets. This study's analysis and presentation greatly benefited from the use of Seaspace Corporation's TeraScan software system and the NCAR Graphics Package.

References

Arking, A., The radiative effects of clouds and their impact on climate. *Bull. Amer. Meteorol. Soc., 71,* 795-813, 1991.

Arking, A., Absorption of solar energy in the atmosphere: Discrepancy between modeled and observations, *Science, 273,* 779-782, 1996.

Barkstrom, B. R., 1984: The Earth Radiation Budget Experiment (ERBE), *Bull. Amer. Meteorol. Soc., 65,* 1170-1185, 1984.

Berliand, T., Methods of climatological computation of total incoming solar radiation, *Meteorol. Gidrol.,* 5, 9-12, 1960.

Bishop, J. K. B., and W. B. Rossow, Spatial and temporal variability of global surface solar irradiance. *J. Geophys. Res., 96,* 16,839-16,858, 1991.

Bishop, J. K. B., W. B. Rossow and E. G. Dutton, Surface solar irradiance from the International Satellite Cloud Climatology Project 1983-1991, *J. Geophys. Res., 102,* 6883-6910, 1997.

Briegleb, B. P., Delta-Eddington approximation for solar radiation in the NCAR Community Climate Model, *J. Geophys. Res., 97,* 7603-7612, 1992.

Brink, N. J., K. A. Moyer, R. P. Trask, and R. A. Weller, The Subduction Experiment: Mooring field program and data summary. *Rep.WHOI-95-08,* 113 pp, Woods Hole Oceanographic Institution, Woods Hole, Mass., 1995.

Cess, R. D., and I. L. Vulis, Inferring surface solar absorption from broadband satellite measurements, *J. Climate, 2,* 974-985, 1989.

Cess, R. D., et al., Interpretation of cloud-climate feedback as produced by 14 atmospheric general circulation models, *Science, 245,* 513-516, 1989.

Cess, R. D., et al., Absorption of solar radiation by clouds: observations versus models, *Science, 267,* 496-499, 1995.

Cess, R. D., M. H. Zhang, Y. Zhou, X. Jing, and V. Dvortsov, Absorption of solar radiation by clouds: Interpretations of satellite, surface and aircraft measurements, *J. Geophys. Res., 101,* 23,299-23,309, 1996.

Charlock, T. P., and T. L. Alberta, The CERES/ARM/GEWEX experiment (CAGEX) for the retrieval of radiative fluxes with satellite data, *Bull. Amer. Meteorol. Soc., 77,* 2673-2683, 1996.

Chou, M. D. and W. Zhou, Estimation and model validation of surface solar radiation and cloud radiative forcing using TOGA COARE measurements. *J. Climate, 10,* 610-620, 1997.

Conant, W. C., V. Ramanathan, F. P. J. Valero and J. Meywerk, An examination of the clear-sky solar absorption over the central equatorial Pacific: Observations versus models, *J. Clim., 10,* 1874-1884, 1997.

Darnell, W. L., W. F. Staylor, S. K. Gupta, N. A. Ritchey and A. C. Wilber, 1992: Seasonal variation of surface radiation budget derived from International Satellite Cloud Climatology Project C1 data, *J. Geophys. Res., 97,* 15,741-15,760, 1992.

Dickey, T., et al., Seasonal variability of biooptical properties in the Sargasso Sea, *J. Geophys. Res., 98,* 865-898, 1993.

Esbensen, S. K. and Y. Kushnir, The heat budget of the global ocean: an atlas based on estimates from surface marine observations. *Rep. 29,* Clim. Res. Inst., Oregon State Univ., Corvallis, 1981.

Ferraro, R., F. Weng, N. Grody, and A. Basist, An eight year (1987-1994) time series of rainfall, clouds, water vapor, snow-cover, and sea-ice derived from SSM/I measurements, *Bull. Amer. Meteorol. Soc., 77,* 891-905, 1996.

Gautier, C., G. Diak, and S. Masse, A simple physical model to estimate incident solar radiation at the surface from GOES satellite data, *J. Clim. Appl. Meteorol., 23,* 1380-1386, 1980.

Grose, W., and J. Gille (Eds), Upper Atmosphere Research Satellite Validation Workshop III Report: Temperature and constituents validation, *NASA Conf. Publ., CP-3317,* 1996.

Gruber, A., and A. F. Krueger, The status of the NOAA outgoing longwave radiation data set, *Bull. Amer. Meteorol. Soc. 65,* 958-962, 1984.

Harshvardhan, R. Davies, D. Randall, and T. Corsetti, A fast radiation parameterization for atmospheric circulation models. *J. Geophys. Res., 92,* 1009-1016, 1987.

Harrison, E. F., P. Minnis, B. R. Barkstrom, V. Ramanathan, R. D. Cess, and G. G. Gibson, Seasonal variation of cloud radiative forcing derived from the Earth Radiation Budget Experiment, *J. Geophys. Res., 95,* 18,687-18,703, 1990.

Herman, J. R., P. K. Bhartia, O. Terres, C. Hsu and C. Seftor, Global distribution of UV-absorbing aerosols from Nimbus 7/TOMS data, *J. Geophys. Res., 102,* 16,911-16,922, 1997.

Hogan, T. F., and T. E. Rosmond, The Description of the Navy Operational Global Atmospheric Prediction System's Spectral Forecast Model. *Mon. Wea. Rev., 119,* 1786-1815, 1991.

Hosom, D. S., R. A. Weller, R. E. Payne, and K. E. Prada, The IMET (Improved Meteorology) Ship and Buoy Systems, *J. Atmos. Oceanic Technol., 12(3),* 527-540, 1995.

Husar, R. B., J. M. Prospero, and L. L. Stowe, Characterization of tropospheric aerosols over the oceans with the NOAA advanced very high resolution radiometer optical thickness operational product, *J. Geophys. Res., 102,* 16,889-16,909, 1997.

Imre, D. G., E. H. Abramson, and P. H. Daum, Quantifying cloud-induced shortwave absorption: An examination of uncertainties and of recent arguments for large excess absroption, *J. Appl. Meteorol., 35,* 1991-2010, 1996.

Intergovernmental Panel on Climate Change (IPCC), *Climate Change 1995, The Science of Climate Change,* edited by J. T. Houghton, L. G. Meira Filho, B. A. Callander, N. Harris, A. Kattenberg, and K. Maskell, Cambridge Univ. Press, New York, 1995.

Jing, X., and R. D. Cess, Comparison of atmospheric clear-sky radiation models to collocated satellite surface measurements in Canada, *J. Geophys. Res., 103,* 28,817-28,824, 1998.

Kalnay, E., et al., NCEP/NCAR 40-year reanalysis project. *Bull. Amer. Meteorol. Soc., 77,* 437-471, 1996.

Kato, S., T. P. Ackerman, E. E. Clothiaux, J. H. Mather, G. G. Mace, M. L. Wesely, F. Murcray, and J. J. Michalsky, Uncertainties in modeled and measured clear-sky surface shortwave irradiances, *J. Geophys. Res., 102,* 25,881-25,897, 1997.

Katsaros, K. B., and J. E. DeVault, On irradiance measurement errors

at sea due to tilt of pyranometers, *J. Atmos. Oceanic Technol., 3,* 740-745, 1986.

Kessler, W.S. and M.J. McPhaden, The 1991-93 El Nino in the Central Pacific, *Deep Sea Res., II, 42,* 295-334, 1995.

Kiehl, J. T., J. J. Hack, M. H. Zhang, and R. D. Cess, Sensitivity of a GCM climate to enhanced shortwave cloud absorption. *J. Clim., 8,* 2200-2212, 1995.

Li, Z., H. G. Leighton, K. Masuda, and T. Takashima, Estimation of SW flux absorbed at the surface from TOA reflected flux, *J. Clim., 6,* 317-330, 1993a.

Li, Z., H. G. Leighton, and R. D. Cess, Surface net solar radiation estimated from satellite measurements: comparisons with tower observations, *J. Clim., 6,* 1764-1772, 1993b.

Li, Z., C. H. Whitlock, and T. P. Charlock, Assessment of global monthly mean surface insolation estimated from satellite measurements using Global Energy Balance Archive data, *J. Clim., 8,* 315-328, 1995.

MacWhorter, M. A., and R. A. Weller, Error in measurements of incoming shortwave radiation made from ships and buoys, *J. Atmos. Oceanic Technol., 8,* 108-117, 1991.

McPhaden, M.J., The Tropical Atmosphere-Ocean array is completed, *Bull. Am. Meteorol. Soc., 76,* 739-741, 1995.

Moyer, K. A., and R. A. Weller, Observations of surface forcing from the Subduction Experiment: A comparison with global model products and climatological datasets, *J. Clim., 10,* 2725-2742, 1997.

Murtagudde, R., and A. J. Busalacchi, Salinity effects in a tropical ocean model, *J. Geophys. Res., 103,* 3283-3300, 1998.

Oberhuber, J. M, An atlas based on the COADS data set. Rep. 15, Max Planck-Inst. fur Meteorol., Hamburg, Germany, 1988.

Ohmura, A., and H. Gilgen, *Global Energy Balance Archive (GEBA). World Climate Program – Water Project A7, Report 2: The GEBA Database, Interactive Application, Retrieving Data*, 60 pp, Verlag der Fachvereine, 1991.

Ohmura, A. et al., Baseline surface radiation network (BSRN/WCRP): New precision radiometry for climate research, *Bull. Am. Meteorol. Soc., 79,* 2115-2136, 1998.

Payne, R. E., Albedo of the sea surface, *J. Atmos. Sci., 29,* 959-970, 1972.

Pilewskie, P., and F. P. J. Valero, Direct observations of excess solar absorption by clouds, *Science, 267,* 1626-1629, 1995.

Pinker, R. and I. Laszlo, Modeling surface solar irradiance for satellite applications on a global scale, *J. Appl. Meteorol., 31,* 194-211, 1992.

Plueddemann, A. J., R. A. Weller, M. Stramska, and T. D. Dickey, Vertical structure of the upper ocean during the Marine Light-Mixed Layers Experiment, *J. Geophys. Res., 100,* 6605-6619, 1995.

Prospero, J. M., Saharan dust transport over the north Atlantic Ocean and Mediterranean: An overview, in *The Impact of Desert Dust Across the Mediterranean,* edited by S. Guerzoni and R. Chester, pp. 133-151, Kluwer Acad. Norwell, Mass., 1996.

Ramanathan, V., B. Subasilar, G. J. Zhang, W. Conant, R. D. Cess, J. T. Kiehl, H. Grassl, and L. Shi, Warm pool heat budget and shortwave cloud forcing: A missing physics? *Science, 267,* 499-503, 1995.

Reed, R. K., On estimating insolation over the ocean, *J. Phys. Oceanogr., 6,* 781-800, 1977.

Rossow, W.B., and R. A. Schiffer, ISCCP Cloud Data Products, *Bull. Am. Meteorol. Soc., 72,* 2-20, 1991.

Rossow, W. B., and Y.-C. Zhang, Calculation of surface and top of atmosphere radiative fluxes from physical quantities based on ISCCP data sets, 2, Validation and first results, *J. Geophys. Res., 100,* 1167-1197, 1995.

Rossow, W.B., A.W. Walker, D.E. Beuschel, and M.D. Roiter, International Satellite Cloud Climatology Project (ISCCP) documentation of new cloud datasets. *Tech. Note WMO/TD-No. 737,* 115 pp., World Meteorol. Org., Geneva, 1996.

Russell, P. B., et al. Global to microscale evolutoin of the Pinatubo volcanic aerosol derived from diverse measurements and analyses, *J. Geophys. Res., 101,* 18,745-18,763, 1996.

Seager, R., and M. B. Blumenthal, Modeling tropical Pacific sea surface temperature with satellite-derived solar radiative forcing, *J. Clim., 7,* 1944-1957, 1994.

Servain, J., A.J. Busalacchi, M.J. McPhaden, A.D. Moura, G. Reverdin, M. Vianna, and S.E. Zebiak, 1998: A Pilot Research Moored Array in the Tropical Atlantic (PIRATA), *Bull. Am. Meteorol. Soc., 79,* 2019-2031, 1998.

Spencer, R. W., Global oceanic precipitation from the MSU during 1979-91 and comparisons to other climatologies, *J. Clim., 6,* 1301-1326, 1993.

Stowe, L. L., R. M. Carey, and P. P. Pelligrino, Monitoring the Mt. Pinatubo aerosol layer with NOAA/11 AVHRR data, *Geophys. Res. Lett., 19,* 159-162, 1992.

Stowe, L. L., A. M. Ignatov, and R. R. Singh, Development, validation, and potential enhancements to the second-generation operational aerosol product at the National Environmental Satellite, Data, and Information Service of the National Oceanographic and Atmospheric Administration, *J. Geophys. Res., 102,* 16,923-16,934, 1997.

Waliser, D. E., B. Blanke, J. D. Neelin, and C. Gautier, Shortwave feedbacks and ENSO: Forced ocean and coupled ocean-atmosphere modeling experiments, *J. Geophys. Res., 99,* 25,109-25,125, 1994.

Waliser, D. E., W. D. Collins and S. P. Anderson, An estimate of the surface shortwave cloud forcing over the western pacific during TOGA COARE, *Geophys. Res. Lett., 23,* 519-522, 1996.

Wang, T., Satellite-derived long term net solar radiation over the global ocean surface: Its relationship to low frequency SST variation and El Nino, Master's thesis, Univ. of Calif., Santa Barbara, 1994.

Weare, B. C., Uncertainties in estimates of surface heat fluxes derived from marine reports over the tropical and subtropical oceans, *Tellus, Ser. A, 41,* 357-370, 1989.

Weare, B. C., P. T Strub, and M. D. Samuel, Marine climate atlas of the Tropical Pacific Ocean. Contribution no. 20, 147 pp., Univ. of California, Davis, 1980.

Weller, R. A., Overview of the Frontal Air-Sea Interaction Experiment (FASINEX): A study of air-sea interaction in a region of strong oceanic gradients, *J. Geophys. Res., 96,* 8501-8516, 1991.

Weller, R. A., and S. A. Anderson, Temporal variability and mean values of the surface meteorology and air-sea fluxes in the western equatorial Pacific warm pool during TOGA COARE, *J. Clim., 9,* 1959-1990, 1996.

Weller, R. A., D. L. Rudnick, R. E. Payne, J. P. Dean, N. J. Pennington, and R. P. Trask, Measuring near-surface meteorology over the ocean from an array of surface moorings in the subtropical convergence zone, *J. Atmos. Oceanic Technol., 7,* 85-103, 1990.

Wentz, F. J., L. A. Mattox, and S. Peteherych, New algorithms for microwave measurements of ocean winds: Applications to SEASAT and the Special Sensor Microwave Imager, *J. Geophys. Res., 91,* 2289-2307, 1986.

Wielicki, B. A., B. R. Barkstrom, E. F. Harrison, R. B. Lee, G. L. Smith, and J. E. Cooper, Clouds and the Earth's Radiant Energy System (CERES): An Earth Observing System, *Bull. Am. Meteorol. Soc., 77,* 853-868, 1996.

Whitlock, C. H., et al., First Global WCRP Shortwave Surface Radiation Budget Dataset, *Bull. Am. Meteorol. Soc., 76,* 905-922, 1995.

Wild, M., A. Ohmura, H. Gilgen, and E. Roeckner, Validation of general circulation model radiative fluxes using surface observations, *J. Clim., 8,* 1309-1324, 1995.

Zender, C. S., S. Pope, B. Bush, A. Bucholtz, W. D. Collins, J. T. Kiehl, F. P. J. Valero, and J. Vitko, Atmospheric absorption during ARESE, *J. Geophys. Res., 102,* 29,901-29,915, 1997.

Zhang, Y.-C., W. B. Rossow, and A. A. Lacis, Calculation of surface and top of atmosphere radiative fluxes from physical quantities based on ISCCP data sets, 1, Method and sensitivity to input data uncertainties, *J. Geophys. Res. 100,* 1149-1165, 1995.

Zhang, G.J., V. Ramanathan, and M.J. McPhaden, 1995: Convection-evaporation feedback in the equatorial Pacific, *J. Clim., 8,* 3040-3051, 1995.

R. D. Cess and D. E. Waliser, Institute for Terrestrial and Planetary Atmospheres, State University of New York, Stony Brook, NY, 11794. (rcess@notes.cc.sunysb.edu; waliser@terra.msrc.sunysb.edu)

R. A. Weller, Woods Hole Oceanographic Institution, Woods Hole, MA, 02543. (rweller@whoi.edu)

(Received November 13, 1998; revised August 24, 1999; accepted August 31, 1999.)